SIMULATIONS OF DEEP OPTICAL AND NEAR INFRARED EXTRAGALACTIC COUNTS

ARATI CHOKSHI and CAROL J. LONSDALE
Infrared Processing and Analysis Center
California Institute of Technology
and Jet Propulsion Laboratory
770 S. Wilson Dr., Pasadena, CA 91125, USA

and

PAOLA MAZZEI and GIANFRANCO DE ZOTTI
Osservatorio Astronomico, Vicolo dell' Osservatorio 5
I-35122 Padova, Italy

March 26, 1993

Abstract

Monte-Carlo simulations of three dimensional galaxy distributions are performed, following the prescription of Chokshi & Wright (1988), to study the photometric properties of evolving galaxy populations in the optical and near infrared bands to high redshifts. Galaxies are spatially distributed according to the spatial two point correlation function in a range of cluster to field environments and in volume elements appropriate to the cosmological model under consideration. Details of individual galaxy properties, including luminosities, morphologies, disk-to-bulge ratios, and size distributions are simulated to match local observed galaxy properties. Galaxies have evolving spectral energy distributions that include both stellar emission and internal dust absorption and re-emission. The simulations result in noiseless two dimensional galaxy distributions on the sky that can be compared to the observed deep images in the blue and near-infrared bands. In this paper, the first of a series, we present our baseline model in which galaxy numbers are conserved, and in which no explicit "starburst" population is included. We use the model in an attempt to simultaneously fit published blue and near infrared photometric and spectroscopic observations of deep fields. We find that our baseline models, with a formation redshift, z_f, of 1000, and H_o=50, are able to reproduce the observed blue counts to b_j =22, independent of the value of Ω_o, and also to provide a satisfactory fit to the observed blue band redshift distributions, but for neither value of Ω_o do we achieve an acceptable fit to the fainter blue counts. In the K-band, we fit the number counts to the limit of the present day surveys only for an $\Omega_o = 0$ cosmology.

We investigate the effect on the model fits of varying the cosmological parameters H_o, the formation redshift z_f, and the local luminosity function. Changing H_o does not improve the fits to the observations. However, reducing the epoch of galaxy formation used in our simulations has a substantial effect. In particular, a model with $z_f \simeq 5$ in a low Ω_o universe improves the fit to the faintest photometric blue data without any need to invoke a new population of galaxies, substantial merging, or a significant starburst galaxy population. For an Ω_o=1 universe, however, reducing z_f is less successful at fitting the blue band counts, and has little effect at all at K.

Varying the parameters of the local luminosity function can also have a significant effect. In particular the steep low end slope of the local luminosity function of Franceschini *et al.* allows an acceptable fit to the $b_j \leq 25$ counts for $\Omega_o = 1$, but is incompatible with $\Omega_o = 0$.

Key Words: faint galaxies, galaxy evolution

1 Introduction

Over the last decade, advances in the sensitivity of two dimensional array detectors have led to phenomenal breakthroughs in the observations of faint galaxies. In the blue band the galaxy surveys probe flux levels that are 5-8 magnitudes fainter than the photographic surveys. The near-infrared arrays have only recently become available, and now allow systematic studies of galaxy populations to $K \simeq 21$ mag. The optical and near infrared surveys probe surface densities of galaxies in excess of 10^5 degree^{-2}. Yet these advancements in observations have not resulted in any consensus on the interpretation of the origin of the faint galaxy populations, or on the cosmological models that the observations favor. For example, modelling of the photometric surveys in the blue and the K-band has pointed to contradictory results: the B-band counts increase steeply beyond $b_j \geq 17$ (Koo & Kron 1992 and references therein) in excess of many quiescently evolving galaxy model predictions, even for an open cosmology that maximises the volume (Maddox *et al.* 1990); on the other hand the K-band counts have been explained by quiescently evolving galaxy populations in an $\Omega_o = 1$ cosmological model; an open universe model or a flat universe with a non-zero cosmological constant would predict too many faint systems (Cowie *et al.* 1993). The spectroscopic surveys in B and K provide further contradictions: for example the redshift distributions of the blue populations are consistent with a non-evolving galaxy distribution (Broadhurst, Ellis and Shanks 1988, Colless *et al.* 1990), at variance with the interpretation of the blue number count data. On the other hand, the redshift-magnitude distributions in the K-band require about a magnitude of luminosity evolution in K (Elston 1992).

Guiderdoni & Rocca-Volmerange (1990, 1991) and Rocca-Volmerange & Guiderdoni (1990) have been able to fit the blue band photometric and redshift data with a self-consistent model by either adopting a low value for Ω and a high value for z_f, or by merging processes. Simultaneous fits of the b_j and K band photometric and redshift data have been achieved (Broadhurst, Ellis & Glazebrook 1992, Carlberg & Charlot 1992, Lacey *et al.* 1993) with a similar appeal to merging, and also to starbursts. Another suggestion has been to invoke a *new* population of galaxies not

seen in the local surveys (Cowie *et al.* 1993, Cole, Treyer & Silk 1992). Again the timing of the bright phase of this new population is adjusted to match the observations, but physical arguments have been put forward that suggest that this scenario might not be unreasonable (Babul & Rees 1992). In contrast, Koo & Kron (1992) use a mix of blue, constant star forming galaxies with a steep low end luminosity function, and a *normal* population modelled by declining star forming rates to model the multi-band number counts and also the redshift distributions. Wang (1991) uses a dusty galaxy model with strong evolution to reproduce the b_j and K number counts while truncating the redshift distribution via internal extinction.

The number of models that have been presented and their differences indicate that the data are degenerate to the number of fitting parameters, therefore successful fits can be obtained by different modellers with different combinations of starting assumptions and values for their many parameters. This makes it very difficult to compare and contrast their results. The problem is exacerbated by the fact that the analytical modelling techniques which are usually used to interpret deep galaxy data are limited in their ability to deal self-consistently with the enormous complexity of the physical processes involved in galaxy evolution.

The situation is further complicated by the fact that the galaxy count data themselves suffer from a lack of consensus - Maddox *et al.* (1990) claim an excess in the galaxy counts over non-evolving model predictions at $b_j \simeq 17$, while Metcalfe *et al.* (1991) claim that the excess does not occur till $b_j > 21$. Thus the models are often based on arbitrary normalisations at the bright end, depending on the survey in question.

Another shortcoming of existing models is that they ignore the 2-dimensional distribution of galaxies on the plane of the sky. These models therefore usually ignore such potentially important effects as the distribution of surface brightness among galaxies, the effect of surface brightness dimming on detectability, confusion and clustering, or they make limited analytical corrections for them.

In this series of papers we take a new modelling approach, designed to address some of the

limitations of earlier models. We have developed Monte-Carlo simulations that can not only incorporate the known properties of local galaxies much better than analytical approaches, but which also for the first time model the 2-D distribution of galaxies on the plane of the sky.

Our philosophy for the Monte-Carlo simulations is to take into account as many of the important physical properties as we can to describe local galaxy populations, and not to limit the variables to the number of observables. While the local observations of galaxies are used to constrain some of these parameters, the less well constrained parameters are treated as variables whose effect on deep galaxy data can be studied. Our aim is to simultaneously study the UV through far-infrared properties of galaxies and carry out direct comparisons with the observed galaxy counts, colors, and redshift distributions. In this paper, we make the simplest and minimum assumptions required to simulate field galaxy distributions, and use the best available quiescent galaxy evolution models which keep track of the metallicity/dust content as the stellar population within the system evolves. Thus the models explicitly take into account the extinction and emission properties of dust as a function of time. The star-burst galaxies that have received so much attention from recent results of blue and far infrared galaxy surveys are explicitly ignored. We will defer the effects of relaxing these minimal assumptions to later papers, which will (1) explore the effects of varying other parameters and of relaxing various initial assumptions; (2) extend the fits to other wavelength regions, beginning with 60μm in the far infrared; (3) and investigate the effects of instrumental noise, sky noise, seeing, confusion, clustering and foreground galaxy extinction on the derived source counts.

The simulation procedure is described in section 2. Section 3 describes the galaxy evolution models. Section 4 presents the results of the b_j and K band simulations and compares to them to the observations. Section 5 contains a discussion of the results. Section 6 summarises our work.

2 The Simulation Procedure

Below we provide a brief description of the modelling technique. The simulations presented here are an extension of those presented by Chokshi & Wright (1988), which contains further details of the Monte-Carlo procedures. The models rely on an understanding of galaxy properties in the local universe, and extrapolate them to higher redshifts based on the chosen cosmological model and passive stellar evolution within galaxies. Thus the models are subject to the uncertainties in the local galaxy observations, for example their colors, morphological distribution, and clustering properties. Also, different libraries in stellar evolutionary tracks, and/or different isochrones adopted for galaxy evolution models influence the results. Models using only stellar tracks entail discontinuities in the photometric evolution of early- type systems as suggested by Charlot & Bruzual (1991). Our model uses a homogeneous set of smooth isochrones defining a continuous sequence in mass and ages covering almost all evolutionary phase. We will discuss these points in more detail in Sect. 3.

2.1 The Distribution on the Sky

The simulations are carried out within an angular area $15' \times 15'$ on the sky. The cosmological parameters H_o, Ω_o and the redshift of galaxy formation z_f are treated as variables. In addition we impose a maximum redshift limit on the resulting simulations of z_{max}=5, to limit file size. The local density of galaxies is determined by integrating the chosen local luminosity function to a minimum luminosity of $10^{-4}L^*$, giving a volume density $n_o = 2.075 \times 10^{-1} h^3$ Mpc^{-3} ($h = H_o/100$) for the luminosity function of Efstathiou, Ellis & Peterson (1988) (see next section for a discussion of the selection of the local luminosity function). The number of galaxies per cluster is assigned according to a power law ranging from $\sim 10^2 - 10^4$ members per cluster with an average of 10^3. The average separation of galaxies within the clusters is based on the spatial two point correlation function given by Peebles (1980) and is independent of redshift. Thus the amplitude of the galaxy correlation function decreases as the background density of galaxies increases at higher z. For individual clusters the clustering length changes according to a power law to simulate tight or

diffuse clusters. The diffuse clusters are large enough to effectively simulate "field" environments. The cluster members are placed at the ends of a random walk process and only those members that fall within the required field of view are considered for further simulations. The clustering procedure is discussed in more detail in Chokshi & Wright (1988).

2.2 The Local Luminosity Function

The local luminosity function (LF) is one of the most important parameters upon which models for deep galaxy samples rest. The function is usually parameterized with a Schechter (1976) form:

$$\Phi = 0.4\phi^* \left[10^{0.4(M^*-M_b)}\right]^{\alpha+1} exp\left[10^{0.4(M^*-M_b)}\right] \quad (1)$$

where ϕ^*, M^* and α define the characteristic space density and the magnitude at the knee of the function, and the slope of the faint end of the function.

In Figure 1 we show several recently published field luminosity functions. The parameters describing these functions are presented in Table 1, except for the composite function of Carlberg and Charlot. There is quite a range in the values of ϕ^*, M^* and α for these functions. If we take this large dispersion as a measure of the uncertainty to which we actually know the true value of these parameters in the local universe then clearly the resulting predicted number counts will have corresponding significant uncertainties. Most modellers seek to limit the uncertainty in at least one LF parameter, ϕ^*, by normalising their models to the bright end of the number counts. In this paper we retain ϕ^* as an independent parameter because there is considerable disagreement in the observed level of the blue number counts at bright magnitudes (Shanks 1990), which of course reflects the uncertainty in ϕ^* itself.

Our approach is to run our simulations using more than one local LF so that we can judge directly the effect on the models of the uncertainty in the local LF. We have selected the LF of Efstathiou *et al.* (1988) as our baseline LF, and also run some simulations using the LF of Franceschini *et al.* (1988), and that of Shanks, as given by Metcalfe *et al.* (1991; see also Shanks 1990). We take these three LFs as representative of the range of values of ϕ^*, M^* and α displayed

in Figure 1. Both the Franceschini and the Shanks functions show a steep faint end slope for their late type, blue systems.

Several studies have found a dependence of LF shape with morphological type or color. The RSA sample of Efstathiou *et al.* shows some evidence for the late type galaxies (later than ScI) to have a fainter M^* by ~ 0.58 magnitude, therefore we have adopted this magnitude difference for ScI and later types for this LF. The distribution into various morphological classes is derived from the Second Reference Catalog of Bright Galaxies (de Vaucouleurs, de Vaucouleurs, & Corwin 1976), and consists of 10% ellipticals, 18% S0s, and 72% spirals.

Franceschini *et al.* (1988) exploited a complete sample of 1671 galaxies with $m_p \leq 14.5$ mag. (or $m_p \leq 14$ mag. in some areas), excluding the Virgo cluster region and objects with $cz < 1000\, km\, s^{-1}$. Their sample was divided into two morphological bins: E/S0 and Spiral/Irregular. We derived Schecter function fits to their early and late type subsamples. The resulting values of M^* are given in Table 1. The early type systems show a flat low luminosity end that is similar to the Efstathiou function, while the slope of the faint end for the late-type systems is steep (cf. Table 1). Integrating these luminosity functions to 17th magnitude in the blue yields the result that 10.8% of galaxies are in the early class and 88.2% are late-type. The local volume density obtained by integrating the LF to the limit of the simulations at $10^{-4}L^*$ is $n_o = 0.9656h^3$, which is ≥ 4 times the density derived from the Efstathiou function.

The luminosity function presented by Shanks (1990) has been divided by them into B-V color bins. The sample is based on the AARS survey of Peterson *et al.* (1986). While the shape of this function bears some resemblence to the Franceschini *et al.* function, there is a difference both in the normalisation of the different galaxy classes and also their luminosity scale. Thus at L* the Shanks function is dominated by ellipticals and S0s (their red class), and the break in the function occurs at systematically *brighter* magnitudes for the later type galaxies. This is in contrast to the results of both Efstathiou *et al.* and Franceschini *et al.*. The density of galaxies derived from this function is ~ 3 times higher than the one used in our baseline model. With this function, the red

E/S0 galaxy class comprises $\sim$ 26%, the intermediate color class (Sa-Sb) comprises $\sim$ 25% and the blue class the remaining $\sim$ 49% of the total population.

2.3 Galaxy Simulations

Simulations of individual galaxies are also carried out in a Monte-Carlo fashion such that the overall distribution in properties follows the assigned empirical or analytical law. Thus, luminosities of galaxies are chosen to follow the selected LF.

The distribution of the disk-to-bulge ratios of spirals is adopted from King & Ellis (1985) and lie between 25-75% for S0s and 1-30% for spirals. Scale sizes are derived from the empirical relation between surface brightness and scale size of Thomsen & Fransden (1983) for ellipticals and bulges. A constant central surface brightness is assumed for spirals to determine their scale size. Galaxy position angles on the plane of the sky are uniformly distributed between 0-180°. The ratio of the major to the minor axis is uniformly distributed between 1-21 for disks, 1-7 for *S0* and bulges, and is determined by the type *E0-E7* for ellipticals, and this in turn fixes the inclinations perpendicular to the plane of the sky.

Each morphological class is assigned a range of galaxy spectral classes which reproduce, at their present age, the range in the observed optical-to-near infrared colors of local galaxies. The galaxy evolution models that we adopt here are discussed in more detail in the following section. For each simulated galaxy the total flux at the rest wavelength corresponding to its redshift and age is derived for the appropriate spectral class. This broadband flux is corrected for an internal inclination dependent extinction at the epoch of observation in the galaxy's rest frame. This flux is then distributed onto the 2 dimensional plane of the sky according to the surface brightness profile of the galaxy, which is a de Vaucouleurs' law for ellipticals and bulges, and an exponential law for disks out to six scale lengths. These fluxes are pixelised on to an array (1800$\times$1800) in the observer's frame. We assume that our galaxies are transparent to background systems, so that fluxes from systems at different redshifts along a given line-of-sight are additive. In a later paper we will investigate the effect of obscuration by foreground galaxies.

The image created by the processes described above is a noise-less, infinite sensitivity image. To truly compare the simulated image with real observational data it is necessary to add the effects of noise, including instrumental and background sky noise, and seeing, and then to extract galaxies from the image using the same techniques that observers do. In approaching the simulated data this way we can directly investigate the effects of selection biases, such as those emphasised by Koo & Kron (1992), and the other two-dimensional effects mentioned in Section 1.

We have chosen to defer this step of the analysis of our models to a later paper of this series. For the current paper we accumulate the number counts, redshift distributions and color distributions from the integrated properties of the simulated galaxies before they are laid down on the 2-dimensional grid. Thus the model distributions discussed in Section 4 are the pre-image model galaxies, not the "observed" model galaxies. The reason for this is that it allows us to compare the model results in this paper much more directly with the results of previously published analytical models. We feel that this is an important first step before proceeding to an analysis of the "observed" simulated galaxies.

3 Synthetic Spectral Energy Distributions

In the following sections we summarize the fundamental assumptions of the model which allows us to derive the broad-band spectrum of galaxies over the whole frequency range, from the UV ($\lambda = 0.125$ μm) to the far-IR ($\lambda = 1000$ μm) (see Mazzei, Xu & de Zotti (1992) for more details), as a function of time since galaxy formation.

3.1 The Chemical Evolution Model

We have adopted Schmidt's (1959) parametrization, wherein the star- formation rate (SFR), $\psi(t)$, is proportional to some power of the fractional mass of gas in the galaxy, $f_g = m_{gas}/m_{gal}$, initially assumed to be unity ($m_{gal} = 10^{11}$ $m_\odot$):

$$\psi(t) = \psi_0 f_g^n \ m_\odot \ \mathrm{yr}^{-1}. \tag{2}$$

We have adopted the case $n = 0.5$, advocated by Madore (1977).

The initial mass function (IMF), $\phi(m)$, has a Salpeter (1955) form:

$$\phi(m)dm = A\left(\frac{m}{\mathrm{m}_\odot}\right)^{-2.35} d\left(\frac{m}{\mathrm{m}_\odot}\right) \qquad m_l \leq m \leq m_u, \tag{3}$$

with $m_u = 100\ \mathrm{m}_\odot$ and $m_l = 0.01\ \mathrm{m}_\odot$.

The influence of a different choice of the power law index, n, for the dependence of the SFR on the gas density has been discussed by Mazzei (1988). The effects of different choices for the IMF and its lower mass limit, m_l, are analysed in Mazzei *et al.* (1992) for late–type systems and in Mazzei, de Zotti & Xu (1993) for early–type galaxies. The general conclusion is that the overall evolution of late–type systems is weakly dependent on n, whereas stronger differences could arise for early–type systems.

In this paper, our baseline model uses the previously cited general assumptions. Disentangling SFR and IMF evolutionary effects from counts and color predictions is deferred to future papers.

The galaxy is assumed to be a closed system, *i.e.* we neglect both winds and inflow of intergalactic gas. Supernova driven galactic winds may well be important during the early evolutionary stages of ellipticals, particularly for lower mass objects (Brocato *et al.* 1990). On the other hand, the extended hot coronae around these galaxies, indicated by X-ray observations (e.g. Trinchieri & Fabbiano 1985), may imply the existence of massive halos, capable of hampering or even of preventing steady galactic winds, or of accretion flows. In any case, a reliable modelling of these effects is very difficult.

Also, the gas is assumed to be well mixed and uniformly distributed. However, we do not assume that recycling is instantaneous, *i.e.* stellar lifetimes are taken into account.

The variations with galactic age of the fractional gas mass $f_g(t)$ [and, through eq. (2), of the SFR, $\psi(t)$] and of the gas metallicity $Z_g(t)$ are obtained by numerically solving the standard equations for the chemical evolution of the Galaxy (Tinsley 1980).

3.2 The Photometric Evolution Model

Synthetic Starlight Spectrum

The synthetic spectrum of stellar populations as a function of the galactic age was derived from the UV to the N band (10.2 μm). The contribution of a stellar generation of age τ to the integrated luminosity in the passband $\Delta\lambda$ is given by:

$$l_{\Delta\lambda}(\tau) = \int_{m_{min}}^{m_{max}(\tau)} \phi(m) 10^{-0.4(M_{\Delta\lambda}(m,\tau)-M_{\odot})} dm \quad \mathrm{L_\odot\, m_\odot^{-1}}, \tag{5}$$

where m is the initial stellar mass, m_{min} is the minimum mass represented in the isochrone, $m_{max}(\tau)$ is the maximum mass of stars still visible at the age τ, *i.e.* the largest mass which has not yet reached the stage of either the final explosion or of the formation of a collapsed remnant, $M_{\Delta\lambda}(m,\tau)$ is the absolute magnitude of a star of initial mass m and age τ, and $M_\odot = 4.72$ is the bolometric luminosity of the sun.

The global luminosity at galactic age t is then obtained as the sum of the contributions of all earlier generations, weighted by the appropriate SFR:

$$L_{\Delta\lambda}(t) = \int_0^t \psi(t-\tau) l_{\Delta\lambda}(\tau)\, d\tau \quad \mathrm{L_\odot}. \tag{6}$$

The number of stars born at each galactic age t and their metallicity are obtained by solving the equations governing the chemical evolution, with the SFR and IMF specified above.

To describe their distribution in the H- R diagram we have adopted the theoretical isochrones derived by Bertelli *et al.* (1990) for metallicities Z=0.001 and Z=0.02, extended by Mazzei (1988) up to 100 $\mathrm{m_\odot}$ and to an age of 10^6 yr. The isochrones include all evolutionary phases from the main sequence to the stage of planetary ejection or of carbon ignition, as appropriate given the initial mass.

Following Sandage (1986) we vary the value of ψ_0 [*eq.* (2)] from 100 to 1 $\mathrm{m_\odot\, yr^{-1}}$ to describe the chemical and photometric properties of the galaxies of different morphological types.

Correction for Internal Extinction

The internal extinction has been taken into account assuming that stars and dust are well mixed. The dust to gas ratio was assumed to be proportional to a power of the metallicity, as in Guiderdoni & Rocca-Volmerange (1987). Further details are given in Mazzei *et al.* (1992).

3.3 Emission from Circumstellar Dust

The mid-IR emission from circumstellar dust shells was assumed to be dominated by OH/IR stars (see Mazzei *et al.* 1992 for a discussion). The spectrum of OH 27.2+0.2 (Baud *et al.* 1985) was assumed to be representative for stars of this class (see also Cox *et al.* 1986). Then the total luminosity of OH/IR stars in the passband $\Delta\lambda$ is given by:

$$L_{OH,\Delta\lambda}(t) = F \int_{t_{AGB}(m_{up})}^{t} d\tau\, \psi(t-\tau) \int_{m_{l,OH}(\tau)}^{m_{u,OH}(\tau)} \phi(m) 10^{-0.4(M_{\Delta\lambda}(m,\tau)-M_{\odot})} dm \quad \mathrm{L}_{\odot}, \qquad (7)$$

where $t_{AGB}(m_{up})$ is the time when, in our model, the first OH/IR stars appear, $m_{l,OH}(\tau)$ ($\geq m_{HeF}$) and $m_{u,OH}(\tau)$ ($\leq m_{up}$) are the minimum and the maximum mass of OH/IR stars of age τ. The coefficient F is determined from the condition that OH/IR stars account for 10% of the observed 12 μm luminosity of our galaxy (Ghosh, Drapatz & Peppel 1986; Boulanger & Pérault 1988). We find $F = 0.05$, in good agreement with Herman & Habing's (1985) estimate.

3.4 Diffuse Dust Emission

The diffuse dust emission spectrum takes into account the contributions of two components: warm dust, located in regions of high radiation field intensity (e.g., in the neighborhood of OB clusters) and cold dust, heated by the general interstellar radiation field.

The model allows for a realistic grain-size distribution and includes PAH molecules (see Xu & De Zotti (1989) and Mazzei *et al.* (1992) for more details). The amount of starlight absorbed and re-emitted by dust is determined at each time using the model for internal extinction mentioned above.

The relative contributions of the warm and cold dust components are also evolving with galactic age: the warm/cold dust ratio is assumed to be proportional to the star formation rate.

3.5 Model Colors and Comparison with Nearby Galaxies

Figure 2 shows the spectral evolution for typical elliptical and spiral models as a function of galaxy age. The adopted ψ_o for this figure are 100 and 10 $M_\odot$ per year respectively. In Figure 3 we illustrate the evolution of the rest frame reddened and unreddened colors $(U-V)$ and $(B-K)$, and $(U-V)_0$ and $(B-K)_0$, of synthetic galaxies with five diffrent values of the initial star formation rate, ψ_0: 3, 10, 20, 35 and 100 $m_\odot yr^{-1}$. Small values of ψ_0 correspond to slow initial star formation and slowly declining star formation rates, therefore we expect them to correspond to late type systems. High ψ_0 values correspond to large star formation rates and rapid declines in SFR with time, *ie.* to early type systems. Figure 4 shows the simulated (B-V) and (V-K) colors in the observed frame as a function of z for the two Ω=0,1 cosmologies assuming H_o=50 and z_f=1000.

The best compilations of optical and near-infrared multiaperture data for nearby galaxies to compare these model colors to are the Reference Catalogs of de Vaucouleurs, de Vaucouleurs and Corwin for UBV data, and the de Vaucouleurs & Longo (1988) (*Catalogue of Visual and Infrared Photometry of Galaxies from* 0.5 μm *and* 10 μm) for longer wavelength data. We have used these heterogeneous sets of multiaperture data for local galaxies to derive colors, aperture corrected to log A/D = 0. The UBV data have been corrected following the RC2 (de Vaucouleurs, de Vaucouleurs & Corwin, 1976), and the growth curves in V and K have been derived from the data in de Vaucouleurs & Longo (1988). All data have been corrected for galactic reddening following the maps of Burstein & Heiles (1984). We grouped galaxies of similar type as follows. We define as $E/S0$ all very-early-type galaxies *i.e.* systems classified with a value of the parameter T, as defined in the RC2, such that $T \leq -1$. Sa galaxies are those characterized by $0 \leq T \leq 1$; Sb: $2 \leq T \leq 3$; Sc: $4 \leq T \leq 6$; and the remaining systems are Irr.

The resulting mean observed colors $< U-V >$, $< V-K >$ and $< B-V >$, as a function of type are shown in the upper panel of Table 2, and the distribution of colors for all systems, and for spiral and irregulars alone, are shown in Figure 5. These mean colors are in good agreement with previous work (Aaronson, (1978); de Vaucouleurs & de Vaucouleurs, (1972); see lower panel

of Table 2).

The range of present day (15 Gyr) simulated reddened colors is in good agreement with the observations. In particular the large dispersion in the observed colors of late-type galaxies (Figure 5) is reproduced by changing the initial star-formation rate ψ_0 by a factor of about 3 from 3 to 10 (Figure 3). The colors of *E* and *S0* galaxies are well matched by the higher ψ_0 models.

As described in Section 2, for the simulations each morphological class must be assigned a range of model galaxy spectral classes, defined by their initial star formation rate, ψ_0. Based on Figures 3 and 5 and Table 2 we selected $50 < \psi_0 < 100$ for ellipticals and galaxy bulges, while the old disk populations of *S0*s have $10 < \psi_0 < 50$, and *Sa-Sd* spiral disks and *Irr*s are described by the range $10 > \psi_0 > 1$.

4 Results

4.1 The Simulated Images

Our standard models comprise $15' \times 15'$ simulations imaged on a 1800×1800 pixel array in each of the broad band b_j and K filters. For the K-band simulation we have used the K-band filter function of Wainscoat & Cowie (1992) while the b_j band filter function was provided by Majewski (1992). In plates I-IV we show the central $5' \times 5'$ of the simulated images with a choice of $H_o = 50$, a galaxy formation epoch z_f=1000, and the Efstathiou LF. Plates I and II show the simluations in b_j and K for Ω_o=0 and III and IV show b_j and K for Ω_o=1. Plates V and VI are the same as plates I and II but for z_f=3. The images are displayed on a logarithmic flux scale.

It is possible to pick out some of the the differences expected in the different cosmological models in these plates. For a fixed z_f the difference in the volume elements dominates the K plates: the larger volume element for the Ω_o=0 cosmology (Plate II) results in higher space densities at all flux densities than in the Ω_o=1 case (Plate IV). In the blue band, evolutionary effects cause the brighter galaxies to appear more numerous for Ω_o=1 (Plate III) but the Ω_o=0 image (Plate I) has more numerous faint galaxies as the volume element effect overshadows evolutionary effects. For a

fixed Ω_o=0, the b_j image with lower z_f (Plate V) shows a larger surface density of bright galaxies compared to the high z_f model (Plate I) due to the younger age in the low z_f model. The lower z_f image at K (Plate VI) has similar surface densities of bright galaxies to the high z_f model (Plate II) due to a less dramatic age effect, but it shows the effect of the lower redshift limit in the lower surface density of faint galaxies.

4.2 Number Counts

The number counts derived from the simulations are shown in Figures 6 to 9. We caution the reader that for simulation count levels below about 100 per square degree the counts are subject to significant statistical uncertainty: a count level of 100 per square degree corresponds to only 6.25 simulated galaxies in the 0.0625 square degrees of the simulated image.

In Figure 6 we show the number count relations derived from the simulated galaxies in the b_j and K bands for our baseline model, which has H_o=50, z_f=1000 and uses the Efstathiou *et al.* LF. We show models for two values of Ω_o. Also shown are the observed number counts from Maddox *et al.* (1990), Lilly *et al.* (1991), and Tyson (1988) in the b_j band and Mobasher, Ellis and Sharples (1986), Glazebrook (1991), Jenkins & Reid (1991), and Gardner (1992) in the K-band. Both the Ω_o models fit the bright $b_j < 22$ counts reasonably well, while the $\Omega_o = 0$ model produces a good agreement to the K-band data to the limit of the faintest survey.

Figure 7 shows the changes in the optical and infrared number count predictions for $H_o = 100$. For the higher H_o, the blue number counts are not affected significantly, while the K-counts are reduced by a factor of 2 in a flat cosmology. This is because it takes time to build a significant red giant population and for a galaxy spectrum to develop a 'red bump'. In this case, for $\Omega_o = 1$ a galaxy at z=1 is only $\simeq$ 2.4 Gyr old, while its age is $\simeq$ 5 Gyr for a $\Omega_o = 0$ cosmology. Hence, the reduction of the K-number counts is due to few galaxies contributing at these brightness levels.

Figure 8 shows the changes in the optical and infrared number count predictions for z_f=3 and 5 respectively. For Ω_o=0, the net effect of decreasing z_f is to increase the counts and cause their

turnover at brighter magnitudes, because the the galaxies are younger and brighter in the later formation epoch models. As expected the effect is larger at shorter wavelengths due to more active star formation in galaxies at the same z. For example, the age of a galaxy at z=1 is 10 Gyr for $z_f = 1000$ compared to 6.6 Gyr for $z_f = 5$, in an $\Omega_o = 0$ cosmology. In a critical universe model, the difference in age is smaller, reducing from $\simeq 4.7$ Gyr to 3.8 Gyr. The results suggest that a low z_f, low Ω_o model produces a good aggreement to the deepest b_j and K-band number count data.

Finally in Figure 9 we show the effect of using the luminosity functions of Franceschini *et al.* and Shanks as compared to the Efstathiou *et al.* function, for $z_f \simeq 1000$. The steeper faint end slope of the Franceschini function results in a divergence of the counts based on this function from those based on the Efstathiou function. This divergence occurs at brighter magnitudes in a flat cosmology because at a given apparent magnitude we are sampling further down the luminosity function for this cosmology and therefore are seeing a larger effect due to the diverging faint end slopes. This increase in the $\Omega_o = 1$ counts accounts for an improved fit for the Franceschini LF to $b_j < 25$ counts. On the other hand the Shanks function results in counts that are similar to those based on the Efstathiou function, producing slightly higher counts for the Ω_o=0 case in both bands, and virtually identical counts for $\Omega_o = 1$. This small change in number counts is accounted for by the similarity in the density of galaxies near the break of the Schechter function and the smaller density of late systems relative to the early galaxies at bright absolute magnitudes. The large number of faint blue systems make their appearance for this function at fluxes just below the observable limits.

From Figures 6 to 9 we can conclude that for an Ω_o=0 model, the blue and K band counts can be fit simultaneously throughout their whole range, whichever of the three LFs is used, but only if z_f is low (<5). The value of H_o is not very important in a low Ω_o model. A high value for z_f significantly underproduces the blue counts for all three LFs. A best fit model for Ω_o=0 could be made with a range of formation epochs between 3 and 5 for either the Efstathiou or the Franceschini function, though such a model would fall a little short of the blue counts fainter than 26th magnitude. Since the Shanks function produces slightly higher overall blue counts, a

composite best fit could be achieved for it for a range of slightly larger z_fs, and this fit would be somewhat better at $b_j > 26$ than possible with the other functions.

The fit to the blue and K band counts is not as good for a critical $\Omega_o = 1$ cosmology. All three LFs significantly underproduce the K counts fainter than 17th magnitude, whatever the value of z_f, while the blue counts are fitted only brighter than 22nd magnitude for the Efstathiou *et al.* and Shanks LFs if z_f is high, and about one magnitude fainter if z_f is low. A better fit to the faintest blue counts is possible with the Franceschini function (to 26th magnitude with a low z_f); however this model may overproduce the brightest blue counts, and is no better than the other functions at fitting the K band data with Ω_o=1. For $\Omega_o = 1$, raising H_o above 50 worsens the fit, especially for the K counts.

4.3 Redshift Distributions

Figure 10 shows the simulated blue band redshift distributions in three magnitude ranges for the baseline model, while Figures 11 to 13 show the effects of changing z_f from 1000 to 5 and of replacing the Efstathiou LF with the Shanks and the Franceshini LFs, respectively. Table 3 shows the means and variances from the different model simulations compared to the observations of Broadhurst *et al.* (1988) and Colless *et al.* (1990) in the range $20 \leq b_j \leq 22.5$.

Within the statistical uncertainties of the simulations, all the models with Ω_o=0, except those with the lowest $z_f = 3$, are in reasonable agreement with the data, showing mean redshifts between $\simeq$0.23 to $\simeq$0.35. The best agreement is achieved with the steep low-end Shanks LF, $\Omega_o = 0$ model, or a Franceshini LF for both the extreme Ω_o models. The Ω_o=1 models are systematically less successful, predicting tails to high redshift that are not observed. The qualitative difference in N(z) between the Ω_o models is a direct outcome of the behaviour of luminosity distance in the two cases; galaxies get dimmer faster as a function of z in a low Ω_o model. Thus in flux limited surveys, one preferentially picks up low z galaxies compared to the $\Omega_0 = 1$ case.

4.4 Magnitude Distributions

Figures 14 to 17 show the distribution in absolute magnitude for the same apparent magnitude bins used for the redshift distributions. We see little variation between the distributions predicted by the various models, except for the extension to faint absolute magnitudes for the Franceschini $\Omega_o = 1$ model, which explains the behaviour of the counts in Figure 9.

4.5 Color Distributions

Figures 18 to 21 show the b_j-K color histograms in different K-bins for comparison with the data of Cowie *et al.* (1993). For all of the models the histograms show a small tendency for galaxies to get bluer at fainter magnitudes. This trend is of about the same magnitude as observed by Cowie *et al.*, and for the $\Omega_o = 1$ models the peak and range of the colors agrees well with the observational data also. The $\Omega_o = 0$, high z_f, model colors are too red on average by about 0.5 magnitudes, in each of the three magnitude ranges. In addition the simulated (B-K) distributions extend too far to the red for the brightest systems. This result is expected since for this cosmology and z_f the K-band counts fit the data while the blue band counts are underproduced. However, the colors are in better agreement with the observations for a low value of z_f (Figure 18), as expected from their number-count distributions. All $\Omega = 1$ models underproduce both the optical and the near infrared counts to yield colors in better agreement with observations.

4.6 Summary of Results

We conclude that for an $\Omega_o = 0$ cosmology a good fit can be obtained to the N(m) data irrespective of which LF is adopted provided the galaxy formation redshift is low $z \simeq 5$. The N(b_j) data rule out the highest z_f model if $\Omega_o = 0$, and the N(B-K) data also favor a low z_f model. However, the spectroscopic data show the best agreement with a high z_f model - and the lowest $z_f = 3$ model is strongly rejected by the data. Thus, a best overall model to fit all the number count, redshift and color data consists of low Ω, $z_f \simeq 5$, and a steep low-end LF like that of Franceschini *et al.* (1988)

or Shanks (1990).

It is more difficult to fit the data with $\Omega_o = 1$. In this case the N(z) data favor a high z_f; the low z_f models produce a higher median redshift and longer tail to high redshift than observed. The N(z) data also favor the Efstathiou or Franceshini LFs over the Shanks LF, as the latter function also produces a tail to high redshift that is not observed. The best fit is obtained for the Franceschini LF, for which the blue N(m) can be fitted to $b_j \sim 26$; however there is evidence that this LF overproduces the brightest counts, and it can fit the K counts only to K=17. If we adopt the Efstathiou LF then the best fits reach only b_j=22 and K=17.

We point out again here that our analysis is based on the simulated galaxies that went into making the fields shown in the plates. Thus, like all previous analytical models of deep galaxy samples, the simulated data do not suffer from many of the observational biases that afflict real data. For example, Koo & Kron (1992) have pointed out that the deep galaxy surveys might be severely biased against high redshift galaxies due to surface brightness dimming, which for a constant signal-to-noise, goes as $(1 + z)^{10}$. Thus, it is likely that the high redshift tail in the simulated $\Omega_o = 1$ models is obliterated in a real observational process. Hence, a direct comparison of our simulated data with observations with real data is not completely fair.

We intend to include sky background, atmospheric seeing, and instrumental noise in the images, to study the resulting observational biases and to subject the simulations to the same processing that the real data go through in a future paper (Chokshi *et al.* 1993).

5 Discussion

We have presented the most detailed two dimensional Monte-Carlo simulations of deep galaxy fields in the blue and near infrared wavelength bands. The aim was to see how far the predictions based on the local, observed, normal galaxy properties, together with the simplest assumption of coeval galaxy formation can come towards reconciling the faint galaxy observations. The results show that, irrespective of the assumed cosmological model, for a high z_f the observed blue band counts

beyond $b_j = 22$ are clearly in excess of the quiescent normal galaxy evolution predictions. These results are in contrast to those found by Guiderdoni & Rocca-Volmerange (1990; GRV), who fit the photometric data over the entire optical band and also the spectroscopic data to $b_j = 22$ with their galaxy evolution models using low Ω with a high z_f. This difference is not due to the differences in the bright end normalisation of the counts since both our counts and those of GRV fit the data at b_j=19.

Two important differences may contribute to the different predictions. First, GRV's standard model includes a UV-hot phase for the elliptical and $S0$ galaxies, which form 35% of their total population. This might enhance their blue count contribution with respect to the present set of models. However, two other differences between GRV's models and ours are likely to cancel this effect. On the one hand GRV adopt a Miller-Scalo IMF while we use a Salpeter IMF. This will result in a stronger UV-rising branch in their models because there is more residual gas. On the other hand GRV adopt the instantaneous recycling approximation, while we do not. Their assumption will lower the UV contribution since it results in a faster gas depletion time and higher metal abundances than our approach.

Secondly, GRV use different libraries of stellar tracks, as discussed by Mazzei *et al.* (1992), in particular for the red giant and later phases. Mazzei *et al.* (1992) made a comparison between their procedure and GRV's, using an Sc model with the same SFR and IMF. They confirmed that the difference in stellar tracks is probably the principle reason for the redness of our models compared to those of GRV.

Cowie *et al.* (1993) found that their K number counts could be fit by an $\Omega = 1$ model, while no cosmology could fit the blue and the K counts simultaneously. Both an open and a flat universe model with a cosmological constant, while providing a better fit to the blue counts, overproduced the K-band data. They achieved a simultaneous fit by introducing a population of blue dwarfs at earlier epochs that disappear locally. We cannot fit the K-band data with $\Omega = 1$, but our $\Omega = 0$ models do account for the K-band counts, implying that our models are too blue compared to Cowie

et al. This is puzzling, however, since the direct comparison of our colors with theirs in Figures 18 to 21 shows a generally fair agreement for all models except the Ω_o=0, high z_f one, which shows *redder* colors than the observational data of Cowie *et al.*. Note that we have not normalised either the blue or K band model N(m) distributions to the observational data therefore this puzzle cannot be explained by a normalisation inconsistency in our simulations.

Koo & Kron (1992) used the observed color-magnitude distribution of galaxies combined with a *no evolution model* to qualitatively reproduce the photometric and spectroscopic properties of faint galaxy populations at optical and near infrared wavelengths. Specifically, their model involved a multiple combination of blue starburst systems and red quiescently evolving galaxy populations along with the color-dependent luminosity function of Shanks (1990) that provides a steep faint end slope to the function for blue galaxies. Koo and Kron's model effectively demonstrates that the observations of faint galaxies are still within the realm of what could plausibly be expected from local populations of galaxies.

On the other hand, Wang (1991) constructed a galaxy evolution model which incorporates dust in galaxies to reconcile all of the optical and infrared data. In his model the dust content in bright galaxies increases with look back time countering the luminosity evolution of their stellar populations, while the low luminosity systems are relatively unaffected by extinction effects and thus increase in luminosity with z. The overall effect of such evolution is to increase the contribution of lower luminosity galaxies with respect to bright galaxies with z, in flux limited surveys, such that both the the increase in the faint blue counts and the shallow redshift distributions are simultaneously satisfied.

Since our models explicitly contain an evolving dust content, tied to the increasing metallicity as a function of time, we expect a similar effect to that treated analytically by Wang. The blue band optical depth for various galaxy types is shown for our models in Figure 22. This figure shows that indeed late-type systems are still increasing in dust content and extinction at the present time, while earlier type systems show a rapid increase in optical depth with increasing lookback time at

recent epochs.

Most other efforts to simultaneously reconcile the blue and the K-band data have required departures from what is observed locally and/or new phenomena. For example, Broadhurst *et al.* (1992) used a combination merging and starburst scenario (this does not conserve the local galaxy density and also invokes starbursting SEDs to explain the *excess* blue counts), Babul & Rees (1992), like Cowie *et al.* (1993), hypothesised disappearing populations of dwarfs synchronised to match the faint blue counts and redshift distributions.

Observational evidence for interaction- or merger-driven starbursts in galaxies came from the IRAS survey. This survey found that, locally, only a small fraction of galaxies ($\sim 2\%$) participate in such phenomena. In all merger scenarios the expectation of galaxy interaction is expected to increase with redshift at a rate somewhere in the range $(1+z)^{\sim 3-6}$. In fact, in the Carlberg & Charlot (1992) model, by z=0.5, the typical depth of the redshift surveys, the luminosity function is already dominated by interaction induced-starburst events, explaining the excess in the counts from $b_j = 21$ to the faintest flux levels. Broadhurst *et al.* (1988) and Colless *et al.* (1990) have modelled their counts in terms of a starburst scenario guided by their observations of higher equivalent widths of OII emission in their deeper surveys compared to the brighter spectroscopic survey of Peterson *et al.* (1986). However, as pointed out by Koo & Kron (1992), the two surveys sample very different luminosity ranges with the Peterson sample confined to the sub-L* regime (see the analyses by Eales (1993)) while the Broadhurst *et al.* and Colless *et al.* observations sample ~L*. Thus the increase in the OII strength is possibly a volume effect, where stronger evolutionary effects are detected in the higher redshift samples. So while invoking galaxy mergers and non-conservation of galaxy number densities is one way of resolving the mystery on the nature of the steep blue counts, it is not necessarily the only possible explanation.

We explored the changes to our results produced by varying three of the most fundamental parameters of our simulations. As we expected, while a variation of H_o does not significantly effect our results, both the epoch of galaxy formation and the shape of the local luminosity function are

critical in the interpretation of the faint galaxy data. In fact, both the observed number counts and the redshift distributions could be explained by a low Ω, low z_f model. Varying z_f and the LLF does not satisfy any observational constraints for any flat cosmological model. Thus a low z_f and/or a steep faint end luminosity function may be sufficient to explain all of the photometric and spectroscopic data without further need to invoke a starbursts or mergers of galaxy populations in a low Ω universe, but not in a flat universe.

The variation in the local luminosity function shows that the steep slope of the Franceschini LF can explain the blue counts to $b_j \simeq 26$ for a high Ω, lowz_f case, but has no effect on impriving the fit at K for this Ω_o. The Shanks function gives the same results for the number counts as the Efstathiou function.

Determinations of space densities of low luminosity galaxies are very uncertain because they rely on nearby samples which are heavily affected by local effects. Random velocities are large scale streaming motions hinder the applicability of the redshift-distance relation; estimates based on group membership or distance indicators such as the Tully-Fisher relation are also controversial. Moreover, the local density of galaxies might be higher or lower than the mean density by an unknown factor. Although the careful analysis by Saunders *et al.* (1990), combining data from several complete samples totalling 2818 galaxies, indicates a relatively low density of low luminosity galaxies, substantially higher values are suggested by the deeper 60μm sample of Lonsdale & Hacking (1989).

Some additional justification for adopting a steep luminosity function comes from the clumped redshift distribution observed in the pencil beam survey of Broadhurst *et al.* (1990). Bahcall (1991) demonstrated that the redshift structures seen in that data originate in the known large-scale superclusters. The luminosity function of galaxies within such structures may well deviate substantially from what is observed in field systems. For example, Sandage, Bingelli & Tammann (1985) found that the luminosity function for galaxies in the Virgo cluster exhibits a steep faint end slope unlike that derived for field galaxies by Efstathiou *et al.* (1988). In our simulations, the

galaxy fields do not explictly contain "field" galaxies. Clusters are made large and diffuse enough to mimic field galaxy separations but they have narrow z distributions and thus show similar levels of clustering as observed in the spectroscopic surveys without a substantial field galaxy fraction. Thus there could be a potential problem in our simulations in sampling local 'field' environments for basing the predictions of deeper surveys - both the space density normalisation and the shape of the faint end of the luminosity function could be wrong if the deep surveys are dominated by clusters.

The compatibility between the observations and the simulation models with a change in z_f or faint end luminosity function cannot necessarily be taken as a proof against either the starburst or merger models. Any of the above combination of parameters and/or new phenomena might be responsible for the deep optical and infrared data. The models do strongly argue that interpreting the faint galaxy observations is a multi-parameter problem that cannot neccesarily be addressed by simpler analytical approaches. For example, our fit of the K-band counts with a low Ω_o model just provides a lower bound to the galaxy numbers expected purely from local phenomena and allows room for further evolution in galaxy counts or their luminosity resulting from merging or starburst scenarios.

It must be emphasised that the simulations presented here are *mass-less*, *i.e.* we have simulated the light distributions of galaxies in model universes whose geometry is governed by the cosmological parameters. Thus the success of a low z_f, $\Omega_o = 0$ model simply favors the larger volume provided by an open geometry. A flat geometrical model can explain the deep galaxy K-band observations if either a non-zero cosmological constant is invoked (Lilly *et al.* 1991) or galaxy number density conservation is abandoned. Both these scenarios produce higher predicted galaxy space densities, the first by increasing the volume element and the second by an increase in the number of galaxies at higher redshifts with galaxy mergers or fading then accounting for the galaxy counts observed locally.

It has been suggested that the light of faint blue galaxies is sufficient to explain all metal

production, and since the redshift surveys show shallow distributions, this must have occured at fairly recent epochs (Cowie 1991). The star formation rate of galaxies in our simulations is a step function that is constant at early epochs and then decreases rapidly. Since 72% of our galaxies are late type with ψ_0=1-10 their metal production (as indicated by their dust content in Figure 22) is a slowly increasing function of time covering a large range of redshifts with the lowest ψ_0 systems still increasing their metal content.

The next step in our study of faint galaxy populations is to include further effects, physical and observational, that might influence the outcome of the simulations. These include a color-luminosity effect and foreground extinction in galaxies that might be potentially important. Less important might be the morphology-density relation, while the question of the slope of the faint end of the galaxy luminosity function, and of morphology-dependent luminosity functions still await observational confirmations before being applied to "field" systems. Missing observatioanl effects include sky, noise, seeing, surface brightness dimmings and their effect on galaxy detection and photometric procedures, effects of confusion etc. These effect might potentially be larger than the second order astrophysical effects.

6 Summary

We have presented detailed two dimensional simulations of deep galaxy fields that rely on extrapolating the local observed properties of galaxies to high redshifts based on passive stellar evolution in galaxies and the assumed geometry of space-time. We find that, under the assumption of conservation in galaxy numbers, the models are strongly constrained by the observations of optical and infrared number counts, their redshift and color distributions. The results favour low Ω_o, low z_f models and are best fit by local luminosity functions that show a steep low luminosity slope.

7 Acknowledgements

We thank Rick Ebert for assistance with optimising the simulation code. The research described in this paper was carried out in part by the Jet Propulsion Laboratory, California Institute of Technology, under a contract with the Nasa Aeronautics and Space Administration. This work was supported in part by NASA contract NAS 7-918.

TABLE 1.

PARAMETERS OF LOCAL LUMINOSITY FUNCTIONS

Reference	Φ^*	M^*	α
Efstathiou *et al.* (1988)	0.00195	-21.18	-1.07
Franceschini *et al.* (1988); Early types	0.0004	-21.1	-1.0
Franceschini *et al.* (1988); Late types	0.0012	-20.9	-1.4
Shanks (1990); E,S0,Sab	0.0012	-20.5	-0.7
Shanks (1990); Sbc	0.0006	-21.4	-1.1
Shanks (1990); Scd/Sdm	0.0004	-21.5	-1.5
de Lapparent *et al.* (1989)	0.00250	-20.7	-1.1
Loveday *et al.* (1992)	0.00175	-21.00	-0.97

Table 2.

COLORS OF NEARBY GALAXIES

Type	U-V	V-K	B-V	σ_{U-V}	σ_{V-K}	σ_{B-V}	N_{U-V}	N_{V-K}	N_{B-V}
E/S0	1.42	3.27	0.94	0.11	0.16	0.09	198	132	198
Sa	1.27	3.18	0.90	0.15	0.29	0.08	70	32	73
Sb	1.00	3.13	0.80	0.22	0.26	0.12	78	22	78
Sc	0.62	3.08	0.62	0.20	0.31	0.13	110	13	110
Irr	0.32	...	0.51	0.20	...	0.12	38	...	38
E/S0	1.42	3.22	0.89	...	...	...	54	54	84
Sa	1.32	3.19	0.83	...	...	...	9	9	22
Sb	1.07	3.17	0.75	...	...	...	9	9	34
Sc	0.82	3.09	0.58	...	...	...	20	20	65
Irr	0.32	2.53	0.42	...	...	...	6	6	24

Table 3.

REDSHIFT DISTRIBUTIONS

	$\langle z \rangle$	σ_z^2
Observations	0.27	0.019
Ω_o=1,z_f=1000, Efstathiou LF	0.35	0.134
Ω_o=0,z_f=1000, Efstathiou LF	0.32	0.026
Ω_o=1,z_f=1000, Franceschini LF	0.23	0.031
Ω_o=0,z_f=1000, Franceschini LF	0.26	0.018
Ω_o=1,z_f=1000, Shanks LF	0.49	0.141
Ω_o=0,z_f=1000, Shanks LF	0.26	0.018
Ω_o=1,z_f=5, Efstathiou LF	0.76	0.546
Ω_o=0,z_f=5, Efstathiou LF	0.36	0.030
Ω_o=1,z_f=3, Efstathiou LF	1.15	0.821
Ω_o=0,z_f=3, Efstathiou LF	0.98	1.216

References

Aaronson, M. 1978, *Astrophys. J.*, **221**, L103

Babul, A., & Rees, M. J. 1992, *Mon. Not. R. Astr. Soc.*, **255**, 346

Bahcall, N. A. 1991, *Astrophys. J.*, **376**, 43

Baud, B., Sargent, A. J., Werner, M. W., & Bentley, A. F. 1985, *Astrophys. J.*, **292**, 628

Bertelli, G., Betto, R., Bressan, A., Chiosi, C., Nasi, E., & Vallenari, A. 1990, *Astr. Astrophys. Suppl.*, **85**, 845

Boulanger, F., & Pérault, M. 1988, *Astrophys. J.*, **330**, 964

Broadhurst, T. J., Ellis, Koo, D. C., & Szalay, A. S. 1990, *Nature*, **343**, 726

Broadhurst, T. J., Ellis, R. S., & Glazebrook, K. 1992, *Nature*, **355**, 55

Broadhurst, T. J., Ellis, R. S., & Shanks,T. 1988, *Mon. Not. R. Astr. Soc.*, **235**, 827

Brocato E., Matteucci, F., Mazzitelli, I., & Tornambé A. 1990, *Astrophys. J.*, **349**, 458

Burstein, D., & Heiles, C. 1984, *Astrophys. J.*, **54**, 33

Carlberg, R. G. & Charlot, S. 1992, *Astrophys. J.*, **397**, 5

Charlot, S., & Bruzual, A. G. 1991, *Astrophys. J.*, **367**, 126

Chokshi, A., & Wright, E. L. 1988, *Astrophys. J.*, **333**, 491

Chokshi, A., Lonsdale, C. J., Majewski, S., Mazzei, P., & De Zotti, G. 1993, in prep.

Colless, M., Ellis, R. S., Taylor, K., & Hook, N. 1990, *Mon. Not. R. Astr. Soc.*, **244**, 408

Cowie, L. L. 1991, *Phys. Script.*, **36**, 102

Cowie, L. L., Gardner, J. P., Hu, E. M., Wainscoat, R. J., & Hodapp, K. W. 1993, preprint

Cole, S., Treyer, M., & Silk, J. 1992, *Astrophys. J.*, **385**, 9

Cox, P., Krügel, E., & Mezger, P. G. 1986, *Astr. Astrophys.*, **155**, 380

de Vaucouleurs, G., & de Vaucouleurs, A. 1972 *Mem. R. Astr. Soc.*, **77**, 1

de Vaucouleurs, G., de Vaucouleurs, A., & Corwin, H. G. 1976, *Second Reference Catalog of Bright Galaxies*,(Austin: University of Texas)

de Vaucouleurs, A., & Longo, G. 1988, *Catalog of Visual and Infrared Photometry of Galaxies*,(Austin: University of Texas)

Eales, S. 1993, *Astrophys. J.*, **404**, 51

Efstathiou, G., Ellis, R. S., & Peterson, B. A. 1988, *Mon. Not. R. Astr. Soc.*, **232**, 431

Elston, R. 1992, in IAU 149, *Stellar Populations in Galaxies*, ed. B. Barbuy, in press

Franceschini, A., Danese, L., De Zotti, G., & Toffolatti, L. 1988, *Mon. Not. R. Astr. Soc.*, **233**, 157

Ghosh, S. K., Drapatz, S., & Peppel, U.C. 1986, *Astr. Astrophys.*, **167**, 341

Gardner, J. P. 1992, Ph.D. thesis, University of Hawaii

Glazebrook, K. 1991, as presented in Gardner's thesis (1992)

Guiderdoni, B., & Rocca–Volmerange, B. 1987, *Astr. Astrophys.*, **186**, 1

Guiderdoni, B., & Rocca Volmerange, B. 1990, *Astr. Astrophys.*, **227**, 362 (GRV)

Guiderdoni, B., & Rocca Volmerange, B. 1991, *Astr. Astrophys.*, **252**, 435

Herman, J., & Habing, H. J. 1985, *Phys.Rep.*, **124**, 255

Jenkins, C. R., & Reid, I. N. 1991, *Astr. J.*, **101**, 1595

King, C. R., & Ellis, R. S. 1985, *Astrophys. J.*, **288**, 456

Koo, D. C., & Kron, R. G. 1992, *Ann. Rev. Astr. Astrophys.*, **30**, 613

Lacey, C., Guiderdoni, B., Rocca-Volmerange, B., & Silk, J. 1993, *Astrophys. J.*, **402**, 1

de Lapparent, V., Geller, M. J., & Huchra, J. 1989, *Astrophys. J.*, **343**, 1

Léger, A., & d'Hendecourt, L. 1987, in *Polycyclic Aromatic Hydrocarbons and Astrophysics*, eds. Léger, A., d'Hendecourt, L., Boccara, N., Reidel, Dordrecht, p.223

Lilly, S. J., Cowie, L. L., & Gardner, J. 1991, *Astrophys. J.*, **369**, 79

Lonsdale, C. J., & Hacking, P. B. 1989, *Astrophys. J.*, **339**, 712

Loveday, J., Peterson, B. A., Efstathiou, G., & Maddox, S. 1992, *Astrophys. J.*, **390**, 338

Madore, B. F. 1977, *Mon. Not. R. Astr. Soc.*, **178**, 1

Maddox, S. J., Sutherland, W. J., Efstathiou, G., Loveday, J., & Peterson, B. A. 1990, *Mon. Not. R. Astr. Soc.*, **247**, 1p

Majewski, S. 1992, *pvt. comm.*

Metcalfe, N., Shanks, T., Fong, R., & Jones, L. R. 1991, *Mon. Not. R. Astr. Soc.*, **249**, 498

Mazzei, P. 1988, Ph. D. Thesis, Intern. School for Advanced Studies, Trieste

Mazzei, P., Xu, C., & De Zotti, G. 1992, *Astr. Astrophys.*, **256**, 45

Mazzei, P., De Zotti, G., & Xu, C. 1993, *preprint*

Mobasher, B., Ellis, R. S., & Sharples, R. M. 1986, *Mon. Not. R. Astr. Soc.*, **223**, 11

Peebles, P. J. E. 1980, *The Large Scale Structure of the Universe*, (Princeton: Princeton Press)

Peterson, B. A., Ellis, R. S., Efstathiou, G., Shanks, T., Bean, A. J., Fong, R., & Zen-Long, Z. 1986, *Mon. Not. R. Astr. Soc.*, **221**, 233

Rocca-Volmerange, B., & Guiderdoni, B. 1990, *Mon. Not. R. Astr. Soc.*, **247**, 166

Salpeter, E. E. 1955, *Astrophys. J.*, **121**, 161

Sandage, A., Binggeli, B., & Tammann, G.A. 1985, *Astr. J.*, **90**, 1759

Sandage, A. 1986, *Astr. Astrophys.*, **161**, 89

Saunders, W., Rowan-Robinson, M., Lawrence, A., Efstathiou, G., Kaiser, N., Ellis, R. S., & Frenk, C. S. 1990, *Mon. Not. R. Astr. Soc.*, **242**, 318

Schmidt, M. 1959, *Astrophys. J.*, **129**, 243

Shanks, T. 1990, *Galactic and Extragalactic Background Radiation*, IAU Symp. 139, ed. S. Bowyer, Ch. Leinert, p.269

Schechter, P. 1976, *Astrophys. J.*, **203**, 297

Tinsley, B. 1980 *Fundam. Cosmic Phys.*, **5**, 287

Thomsen, B., & Fransden, S. 1983, *Astr. J.*, **88**, 789

Trinchieri, G., & Fabbiano, G. 1985, *Astrophys. J.*, **296**, 447

Tyson, A. J. 1988, *Astr. J.*, **96**, 1

Wainscoat, R. J, & Cowie, L. L. 1992, *Astr. J.*, **103**, 332

Wang, B. 1991, *Astrophys. Lett.*, **383**, L37

Xu, C., & De Zotti, G. 1989, *Astr. Astrophys.*, **225**, 12

Figure Captions

Figure 1: A comparison of different local luminosity functions. dash-triple dot line: Efstathiou, Ellis and Peterson (1988); lower solid line: Shanks (1990); upper solid line: Franceschini *et al.* (1988); dash-dot line: de Lapparent, Geller and Huchra (1989); dotted line: Loveday *et al.* (1992); dashed line: Carlberg and Charlot (1992).

Figure 2: Elliptical (light line) and spiral (heavy line) galaxy photometric evolution models as a function of age.

Figure 3: Rest frame (B-K) and (U-V) colors as a function of age for the galaxy evolution models for different values of the initial star formation rate ψ_0. $(B\text{-}K)_o$ and $(U\text{-}V)_o$ represent the extinction corrected colors. Long dash-dot line: $\psi_0 = 100\ m_\odot\,yr^{-1}$; long dash - short dash line: $35\ m_\odot\,yr^{-1}$; short dash-dot line: $20\ m_\odot\,yr^{-1}$; dashed line: $10\ m_\odot\,yr^{-1}$; solid line: $3\ m_\odot\,yr^{-1}$.

Figure 4: (B-V) and (V-K) colors in the observers frame for galaxy evolutionary models with different initial star formation rates (as in Figure 3) as a function of redshift. Panels (a) and (b) are for $\Omega_o = 1$, and panels (c) and (d) are for $\Omega_o = 0$. z_f=1000 and H_o=50 are assumed for both cases.

Figure 5: Histograms of the observed galaxy (B-V) and (V-K) colors for all morphological types (panels a and b) and for the late type galaxies (panels c and d). The data is derived from a heterogeneous sample, as described in the text.

Figure 6: $N(b_j)$ and N(K) per square degree per magnitude derived from the simulations for our baseline model with z_f=1000 and H_o=50 (lines), for two values of Ω_o. The symbols are the observed number counts. Blue Data: solid squares: Tyson 1988; solid triangles: Metcalfe *et al.* 1991; open squares: Maddox *et al.* 1990; open stars: Lilly *et al.* 1991. K band data: solid circles, open circles, open squares, open stars: Various surveys as reported by Gardner 1992 ;open triangles: Glazebrook 1991; plain error bars: Jenkins and Reid 1991.

Figure 7: Same as Figure 6, illustrating the effect of changing H_o from 50 to 100. The baseline model with H_o=50 is shown as the light lines for two values of Ω_o, while the H_o=100 model is shown as the dark lines.

Figure 8: Same as Figure 6, illustrating the effect of changing the epoch of galaxy formation. For this figure we have put the results for the two values of Ω_o into different panels for the sake of clarity. The baseline model with H_o=50 and z_f=1000 is shown as the solid line in each panel.

Figure 9: Same as Figure 6, illustrating the effect of different local luminosity functions. In this figure the results for the two values of Ω_o are again shown in each panel, with the solid lines for Ω_o=1 and the dashed lines for Ω_o=0. The baseline model with H_o=50, z_f=1000 and the Efstathiou *et al.* (1988) luminosity function is depicted as the light pair of lines in each panel. The other luminosity functions are depicted with the heavier lines.

Figure 10: N(z) per square degree distributions in three b_j magnitude ranges for each value of Ω_o for our baseline model.

Figure 11: Same as Figure 10 but for z_f=5.

Figure 12: Same as Figure 10 , but for the Franceschini *et al.* (1988) luminosity function

Figure 13: Same as Figure 10, but for the Shanks (1990) luminosity function.

Figure 14: Absolute magnitude distributions for the same apparent magnitude ranges used in Figure 10, for our baseline model.

Figure 15: Same as Figure 14 but for z_f=5.

Figure 16: Same as Figure 14 , but for the Franceschini *et al.* (1988) luminosity function

Figure 17: Same as Figure 14, but for the Shanks (1990) luminosity function.

Figure 18: (B-K) colors in different K magnitude ranges for the baseline model.

Figure 19: Same as Figure 18, but for z_f=5.

Figure 20: Same as Figure 18, but for the Franceschini *et al.* (1988) luminosity function.

Figure 21: Same as Figure 18, but for the Shanks (1990) luminosity function.

Figure 22: Face-on blue band optical depth of model galaxies as a function of age, for five different values of the initial star formation rate ψ_0.

Plate I: Central $5' \times 5'$ of simulated b_j band image with H_o = 50 km/s/Mpc, Ω_o=0, z_f=1000 and the Efstathiou *et al.* (1988) luminosity function.

Plate II: Central $5' \times 5'$ of simulated K band image with H_o = 50 km/s/Mpc, Ω_o=0, z_f=1000 and the Efstathiou *et al.* (1988) luminosity function.

Plate III: Central $5' \times 5'$ of simulated b_j band image with H_o = 50 km/s/Mpc, Ω_o=1, z_f=1000 and the Efstathiou *et al.* (1988) luminosity function.

Plate IV: Central $5' \times 5'$ of simulated K band image with H_o = 50 km/s/Mpc, Ω_o=1, z_f=1000 and the Efstathiou *et al.* (1988) luminosity function.

Plate V: Central $5' \times 5'$ of simulated b_j band image with H_o = 50 km/s/Mpc, Ω_o=0, z_f=3 and the Efstathiou *et al.* (1988) luminosity function.

Plate I: Central $5' \times 5'$ of simulated K band image with H_o = 50 km/s/Mpc, Ω_o=0, z_f=3 and the Efstathiou *et al.* (1988) luminosity function.

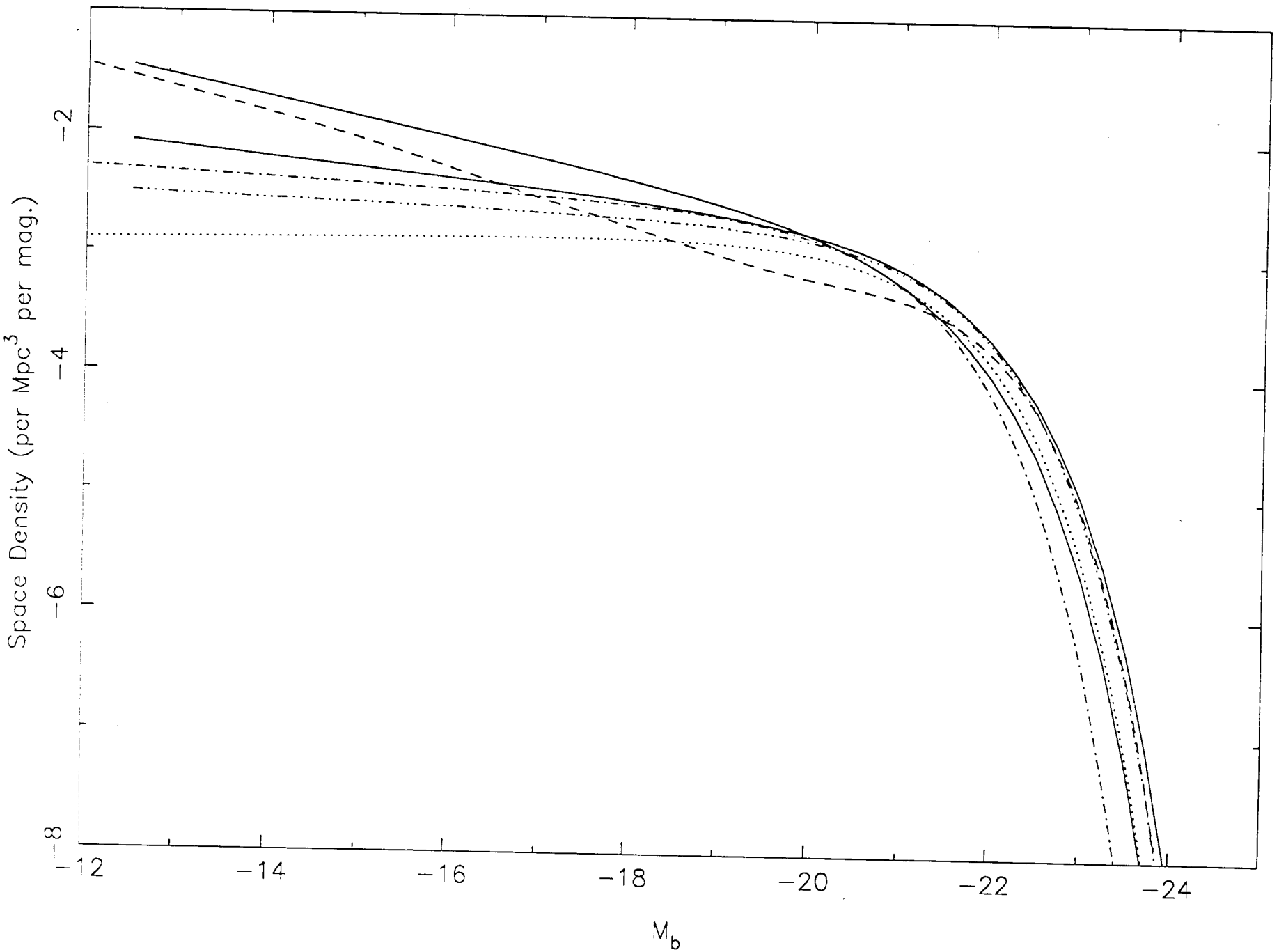

cil 25-Mar-1993 13:48

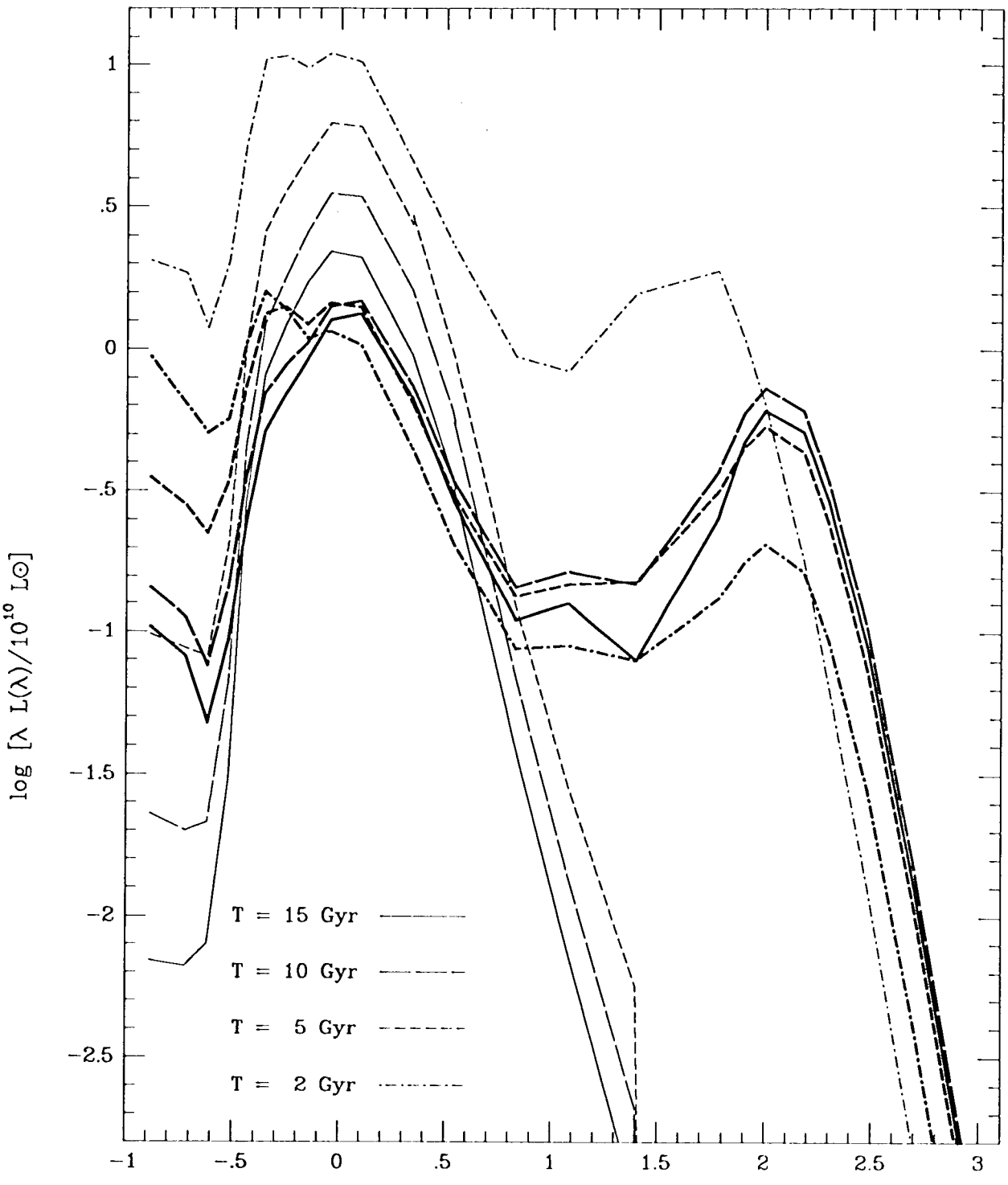
1
.5
0
-.5
-1
-1.5
-2
-2.5
-1
-.5
0
.5
1
1.5
2
2.5
3
log [λ L(λ)/10^10 L⊙]
log λ (μm)
T = 15 Gyr
T = 10 Gyr
T = 5 Gyr
T = 2 Gyr

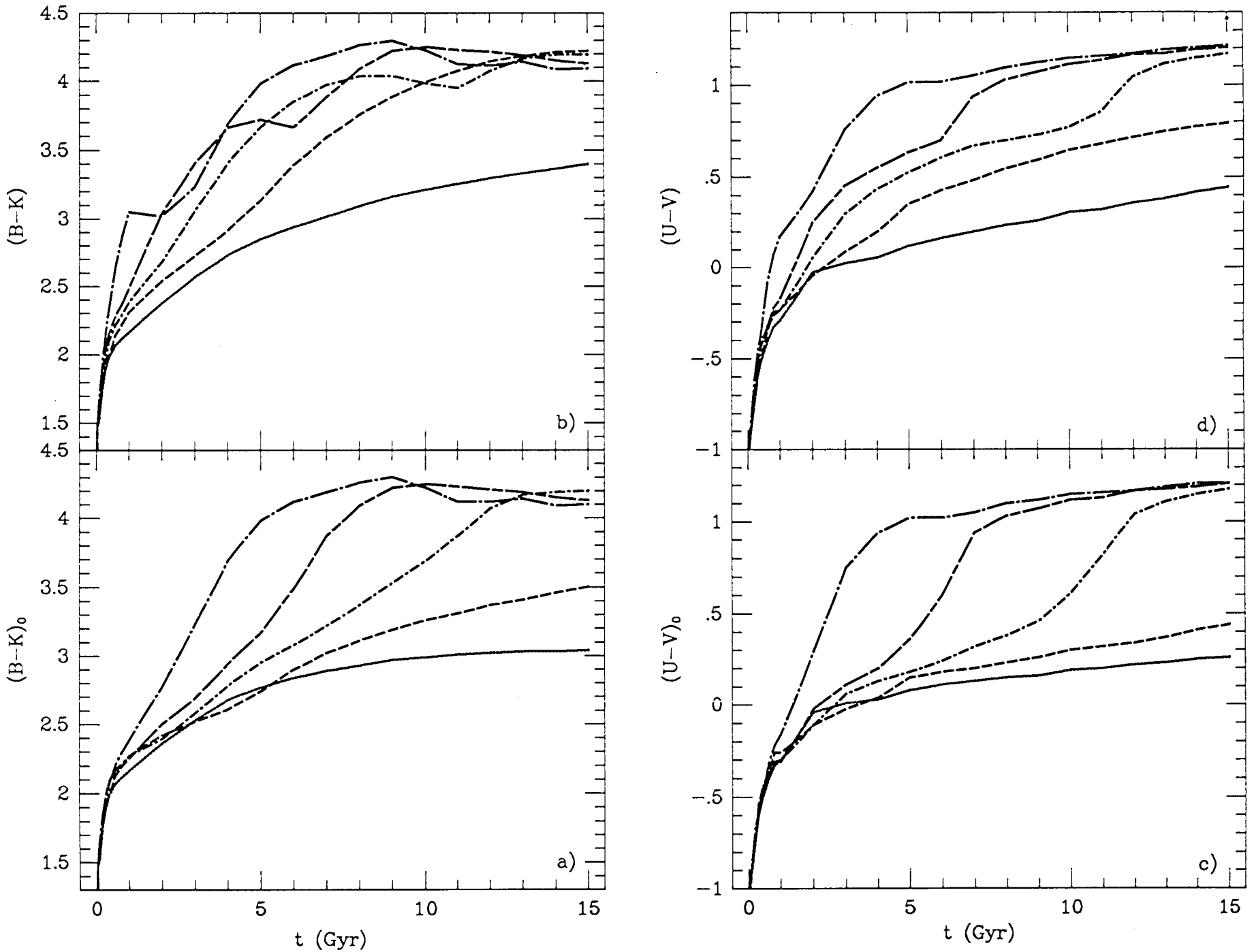
(B−K)
(B−K)₀
(U−V)
(U−V)₀
t (Gyr)
t (Gyr)
a)
b)
c)
d)

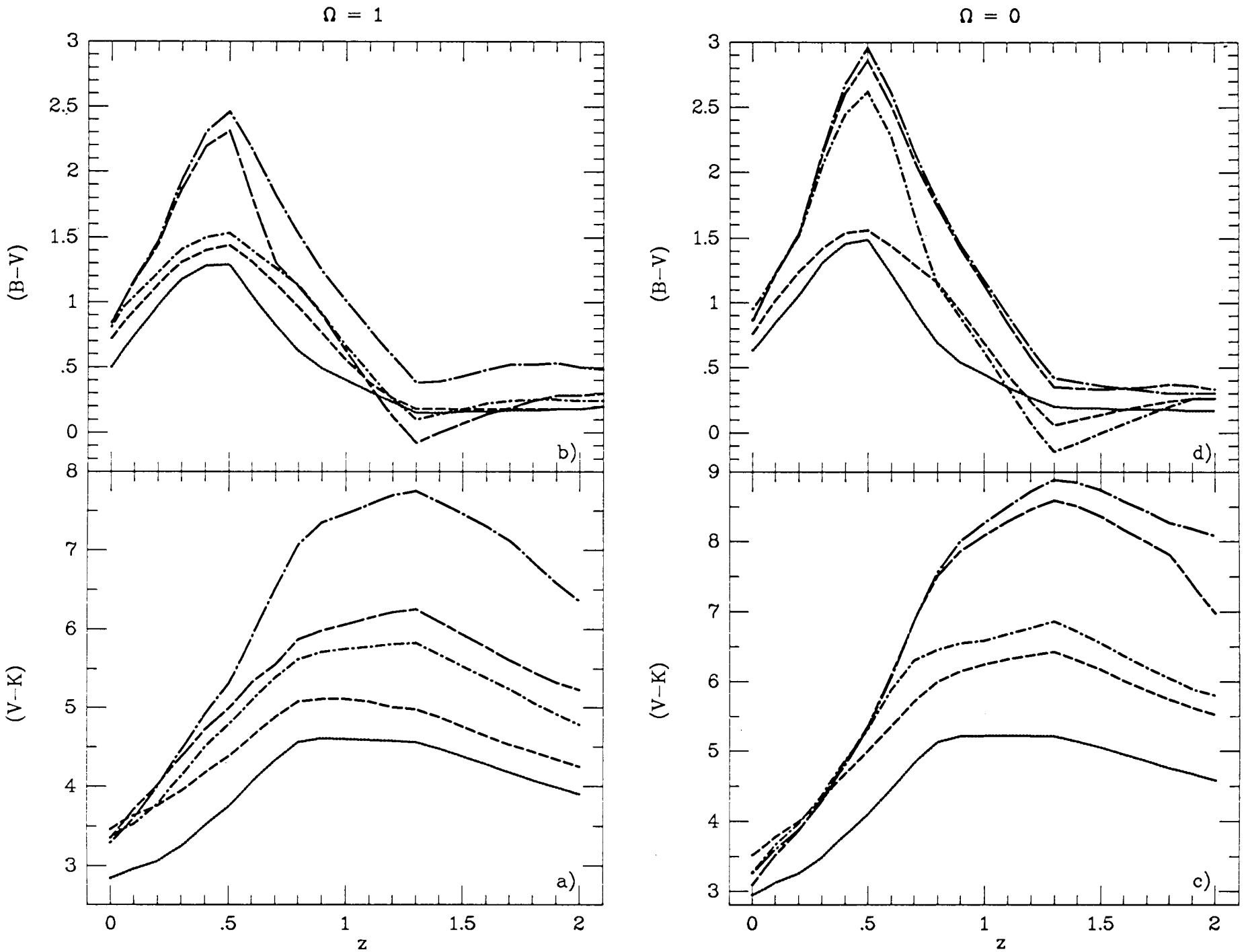
Ω = 1
Ω = 0
(B−V)
(V−K)
z
a)
b)
c)
d)

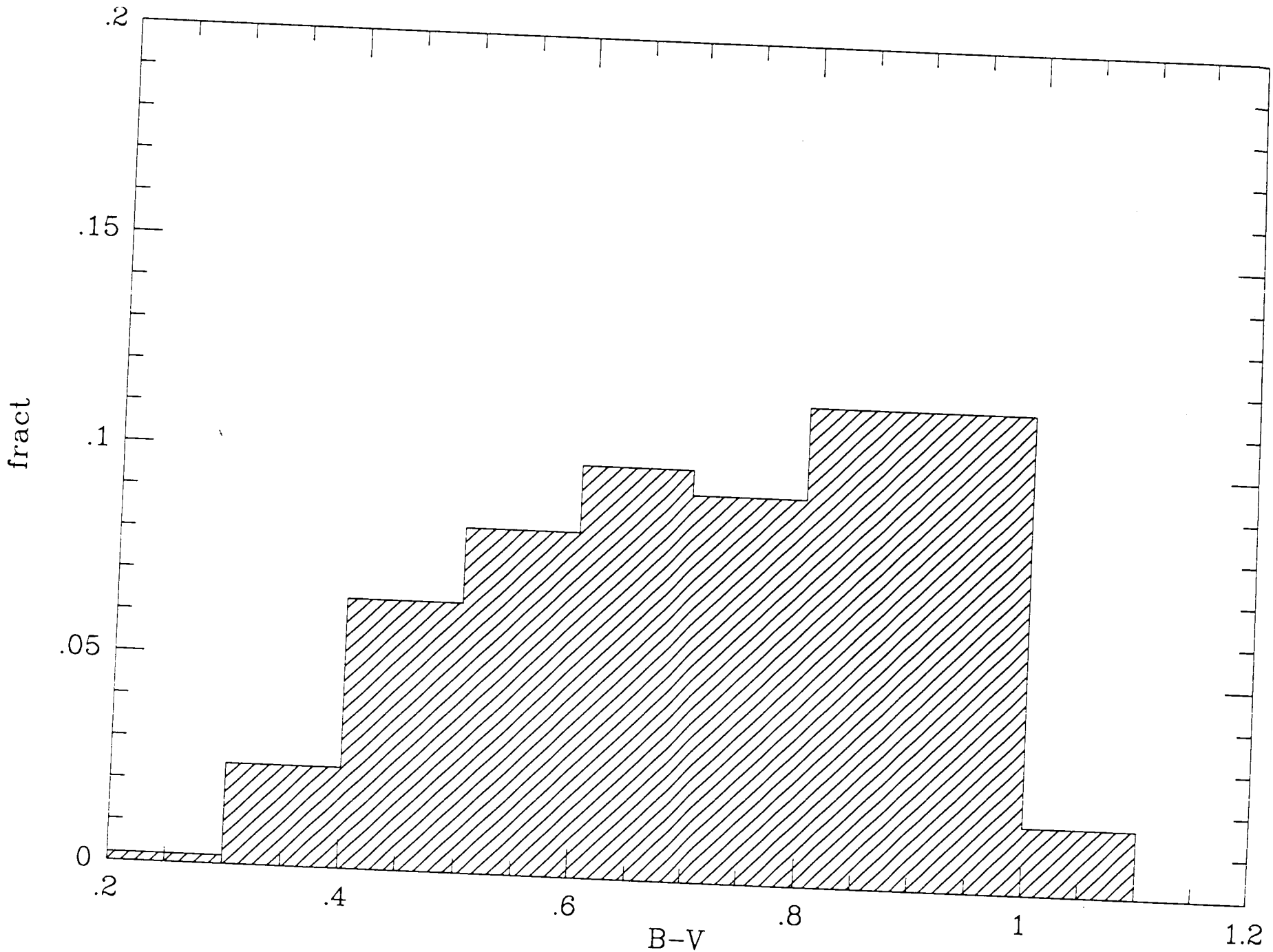
.2
.15
.1
.05
0
fract
.2
.4
.6
.8
1
1.2
B-V

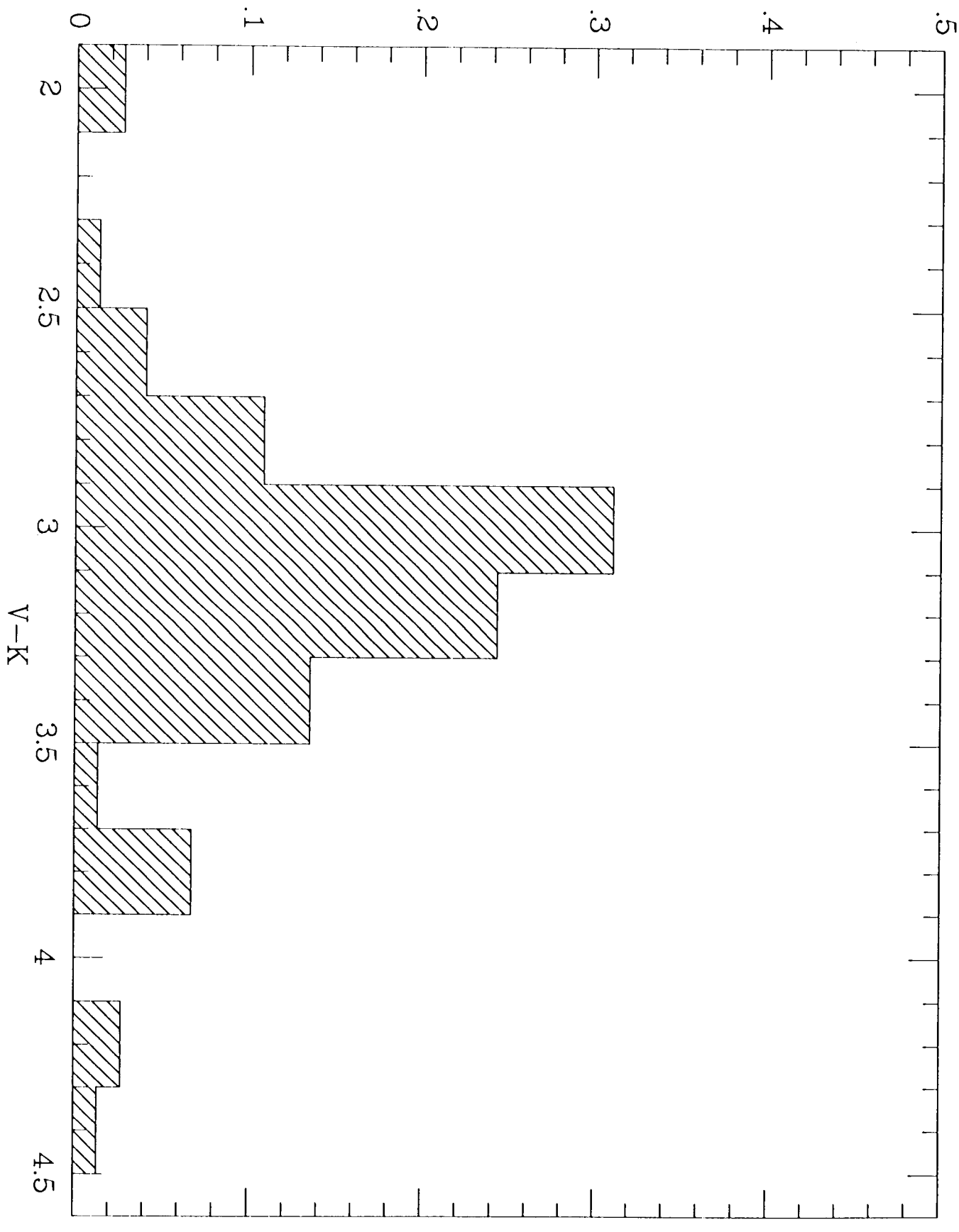
fract
0
.1
.2
.3
.4
.5
2
2.5
3
3.5
4
4.5
V−K

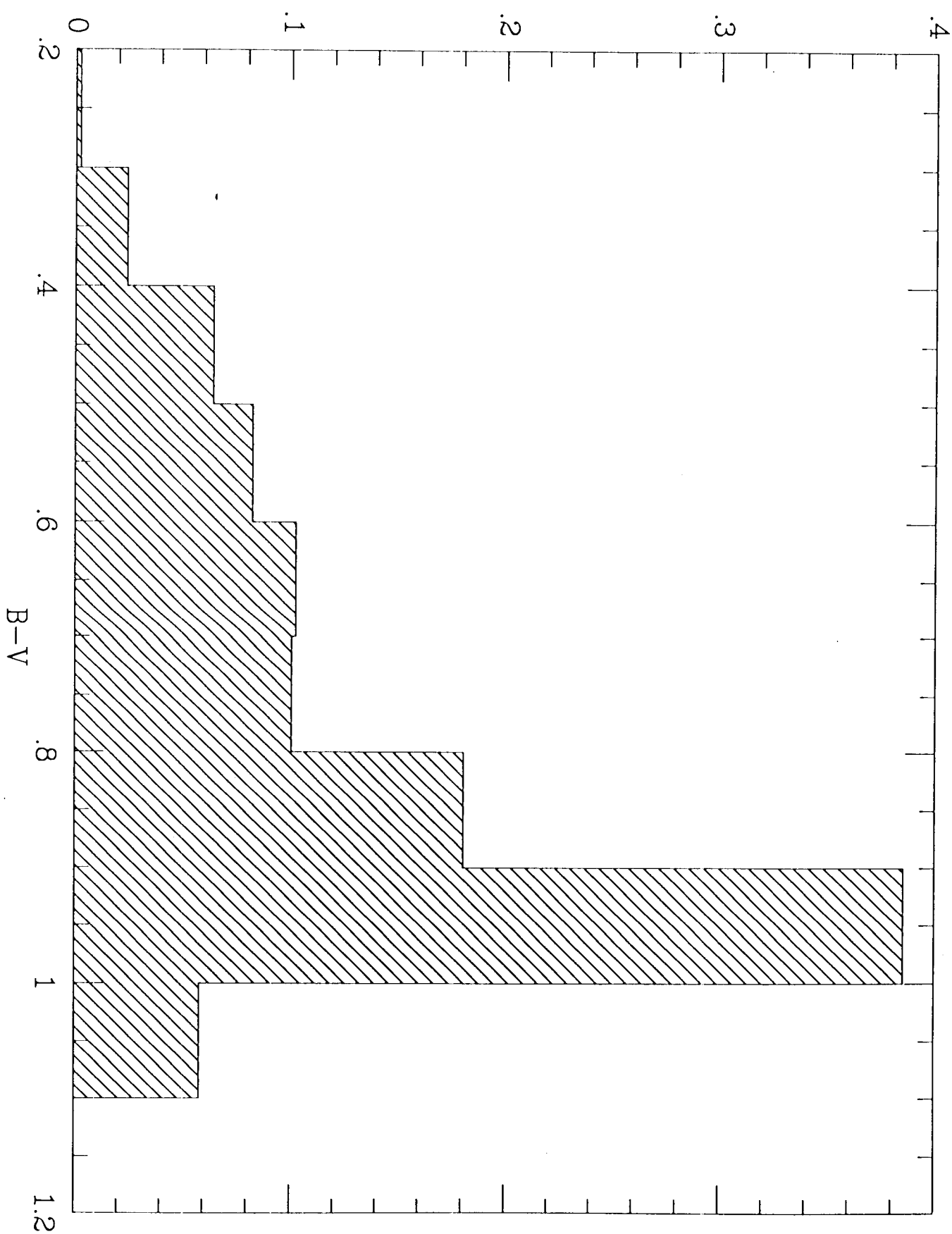
fract
0
.1
.2
.3
.4
.2
.4
.6
.8
1
1.2
B–V

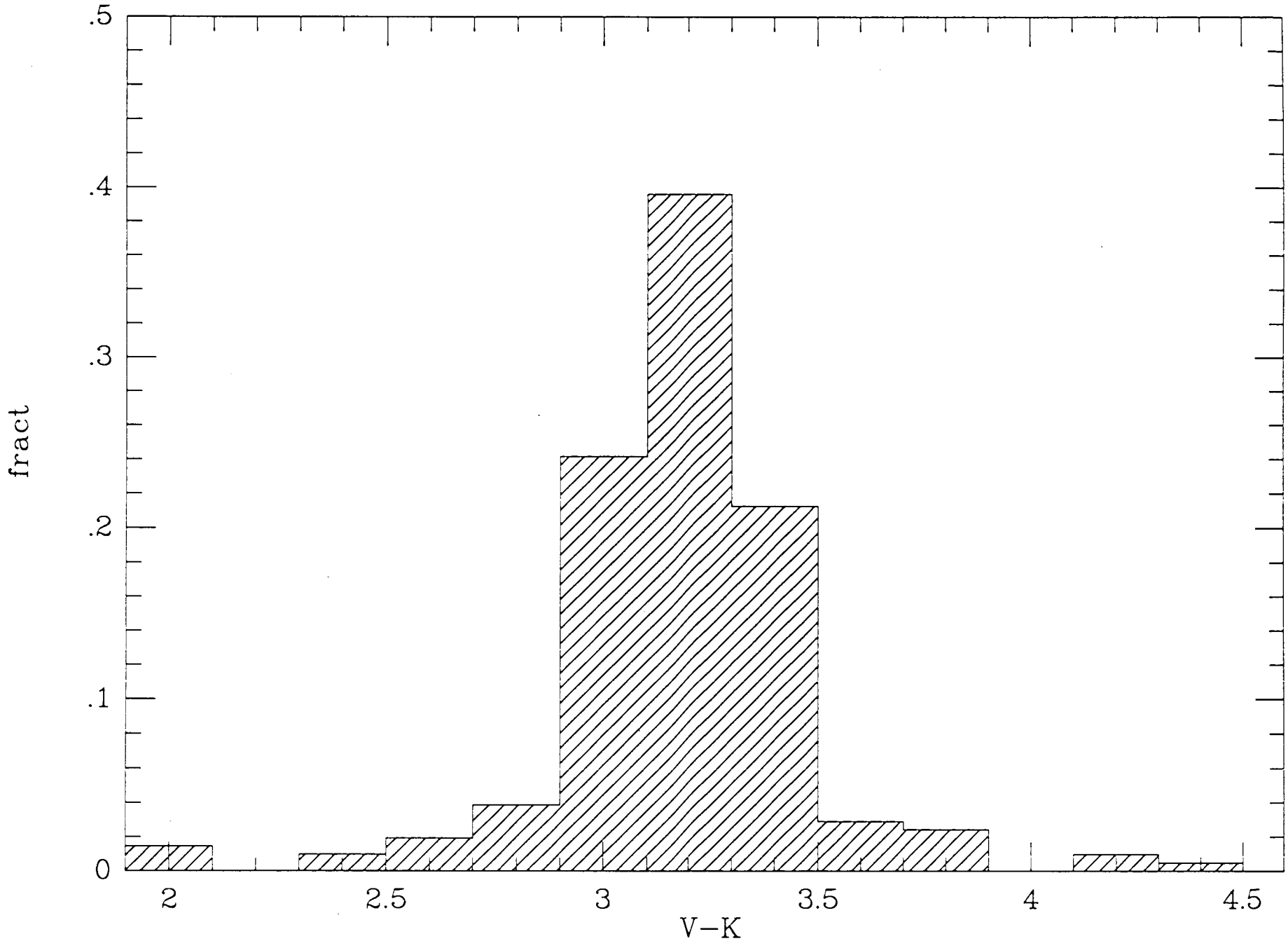
.5
.4
.3
.2
.1
0
fract
2
2.5
3
3.5
4
4.5
V−K

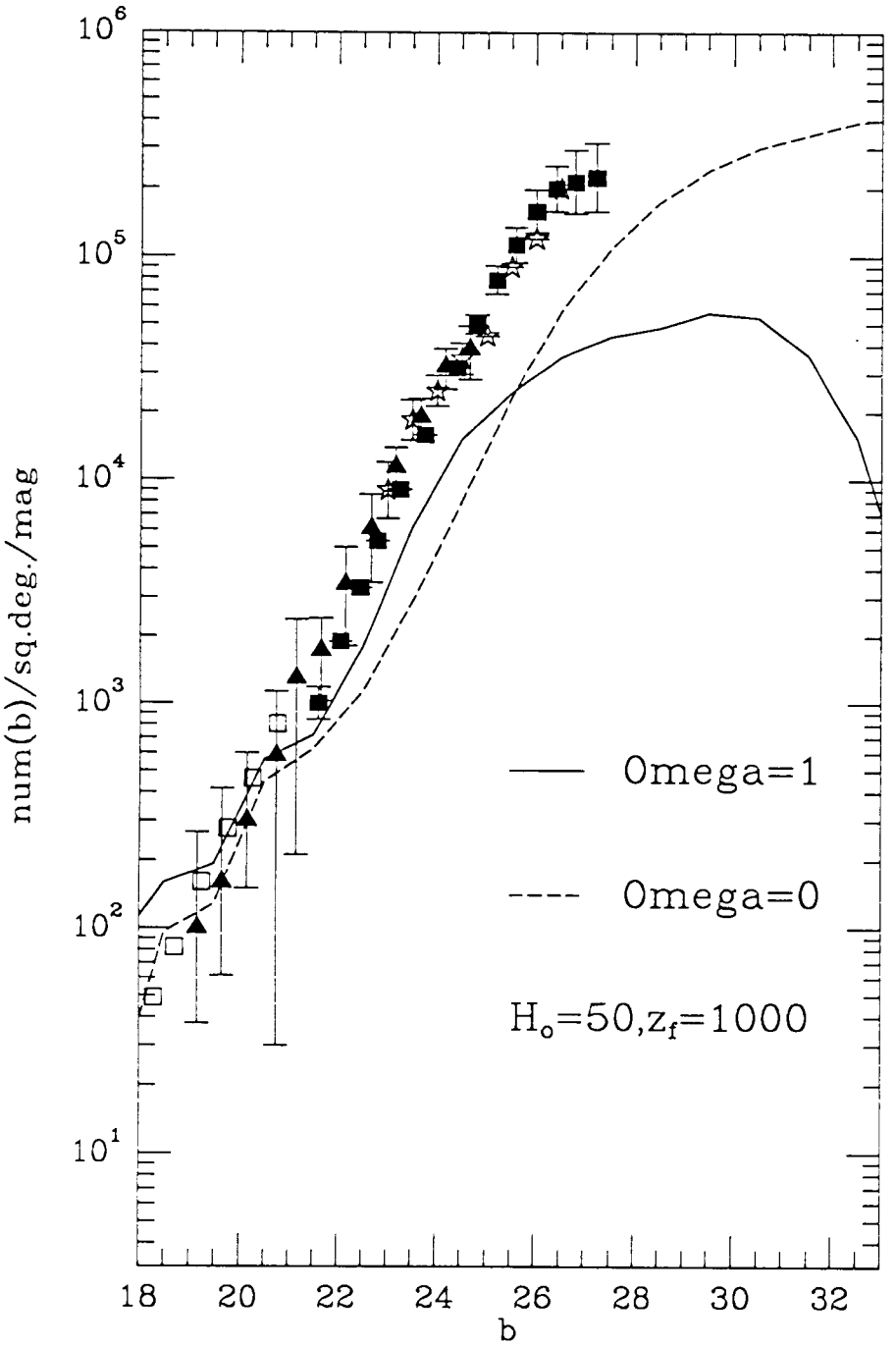
num(b)/sq.deg./mag
b
Omega=1
Omega=0
H_o=50,z_f=1000

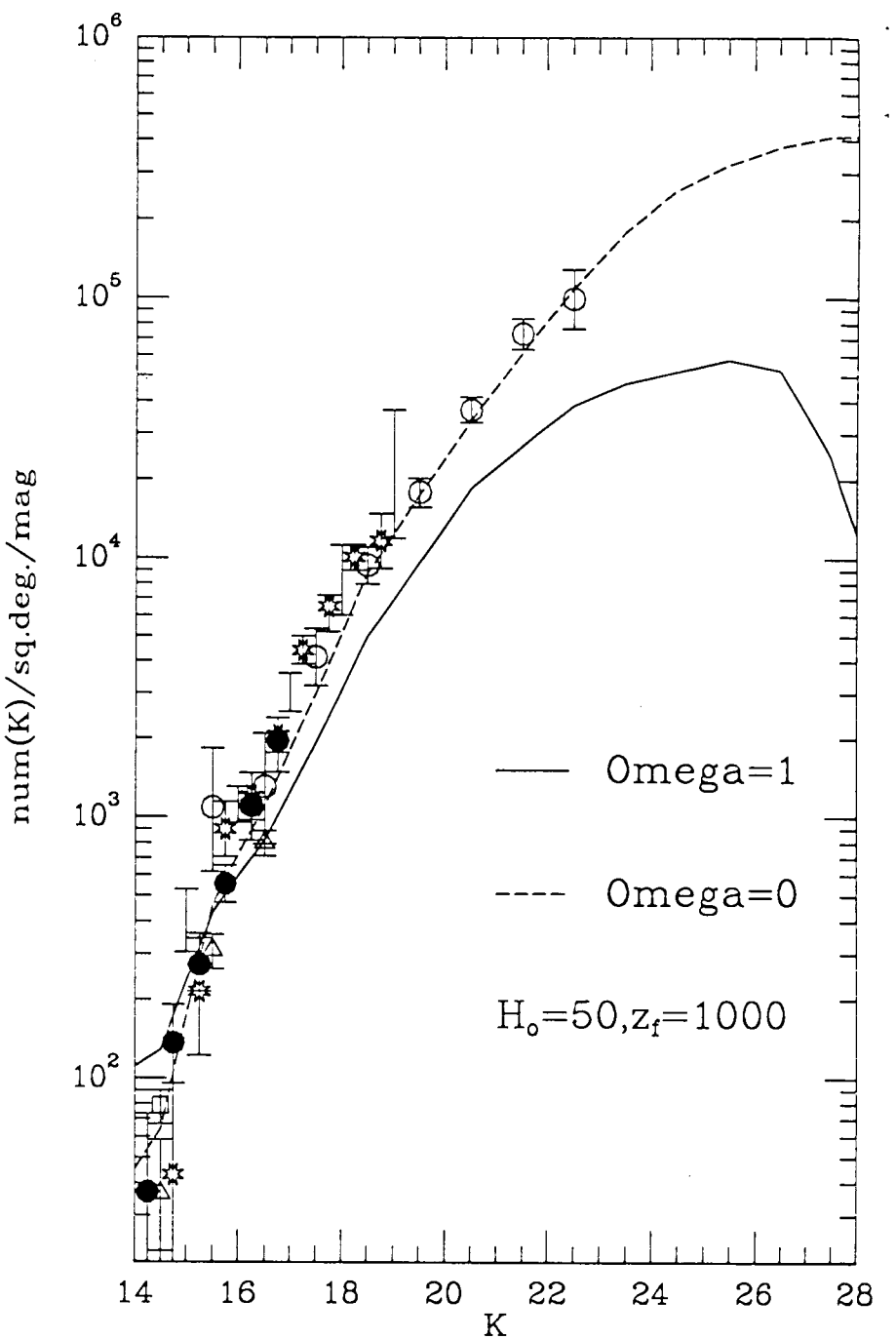
num(K)/sq.deg./mag
K
Omega=1
Omega=0
H_o=50,z_f=1000

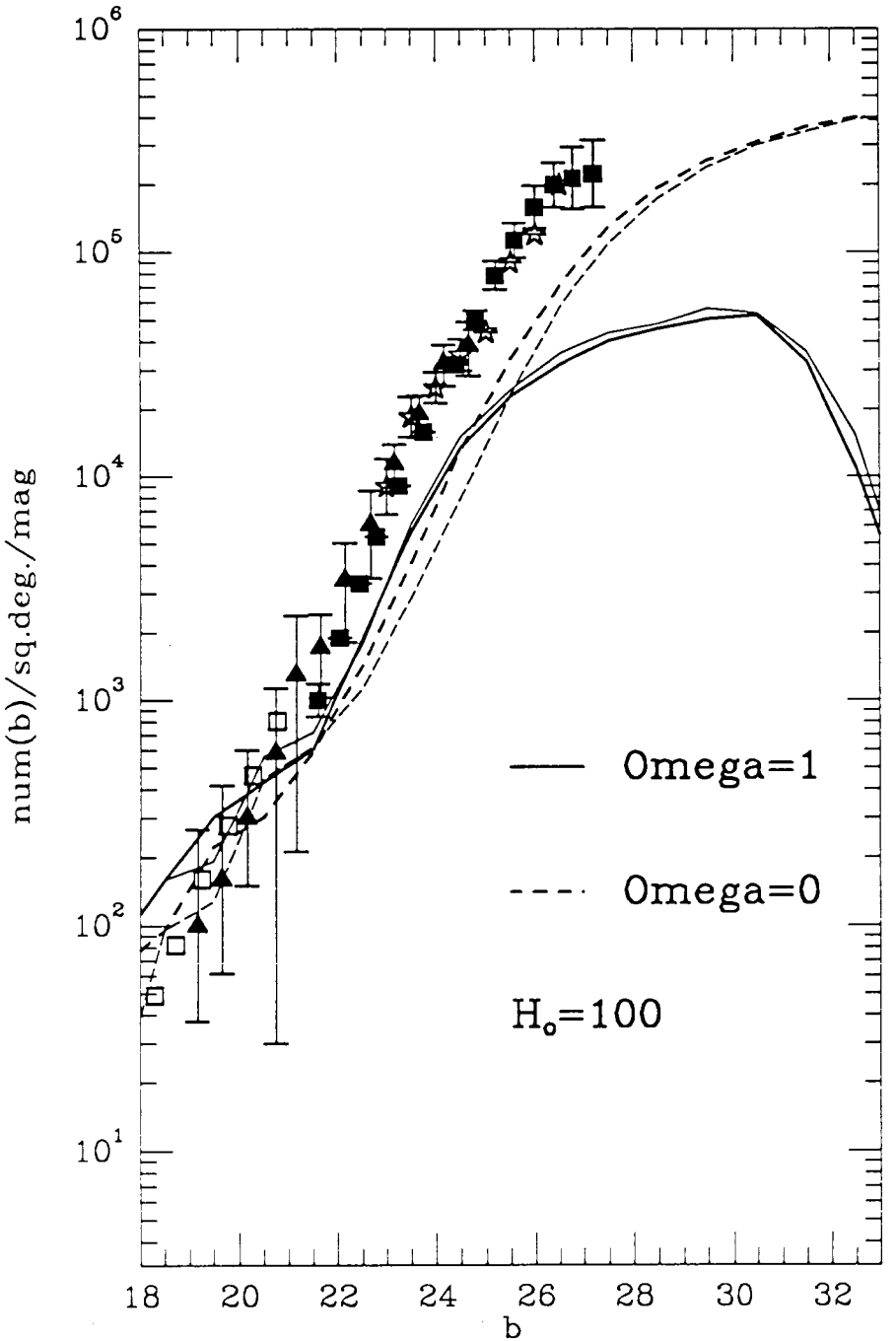
num(b)/sq.deg./mag
b
Omega=1
Omega=0
H$_o$=100

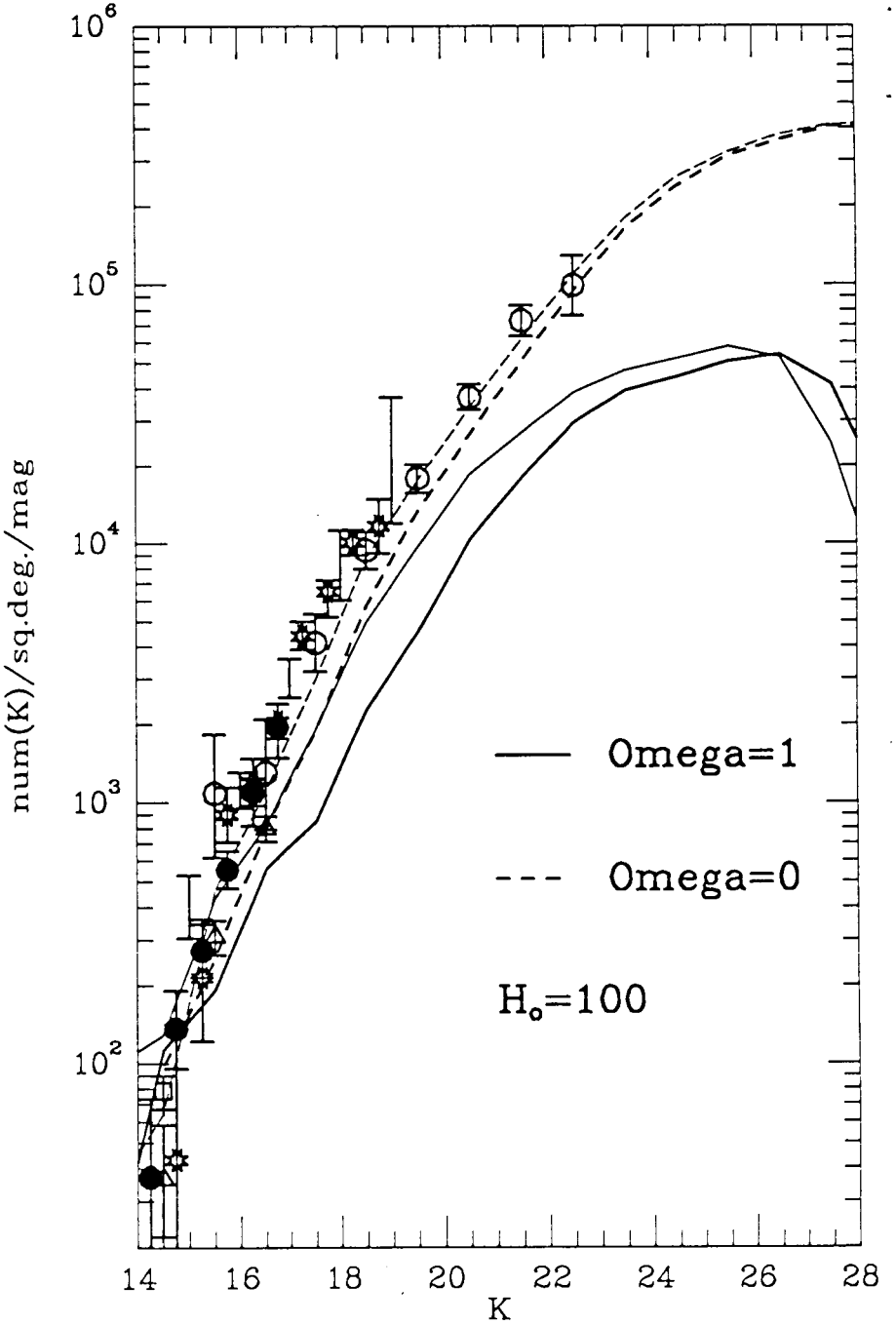
num(K)/sq.deg./mag
K
Omega=1
Omega=0
H$_o$=100

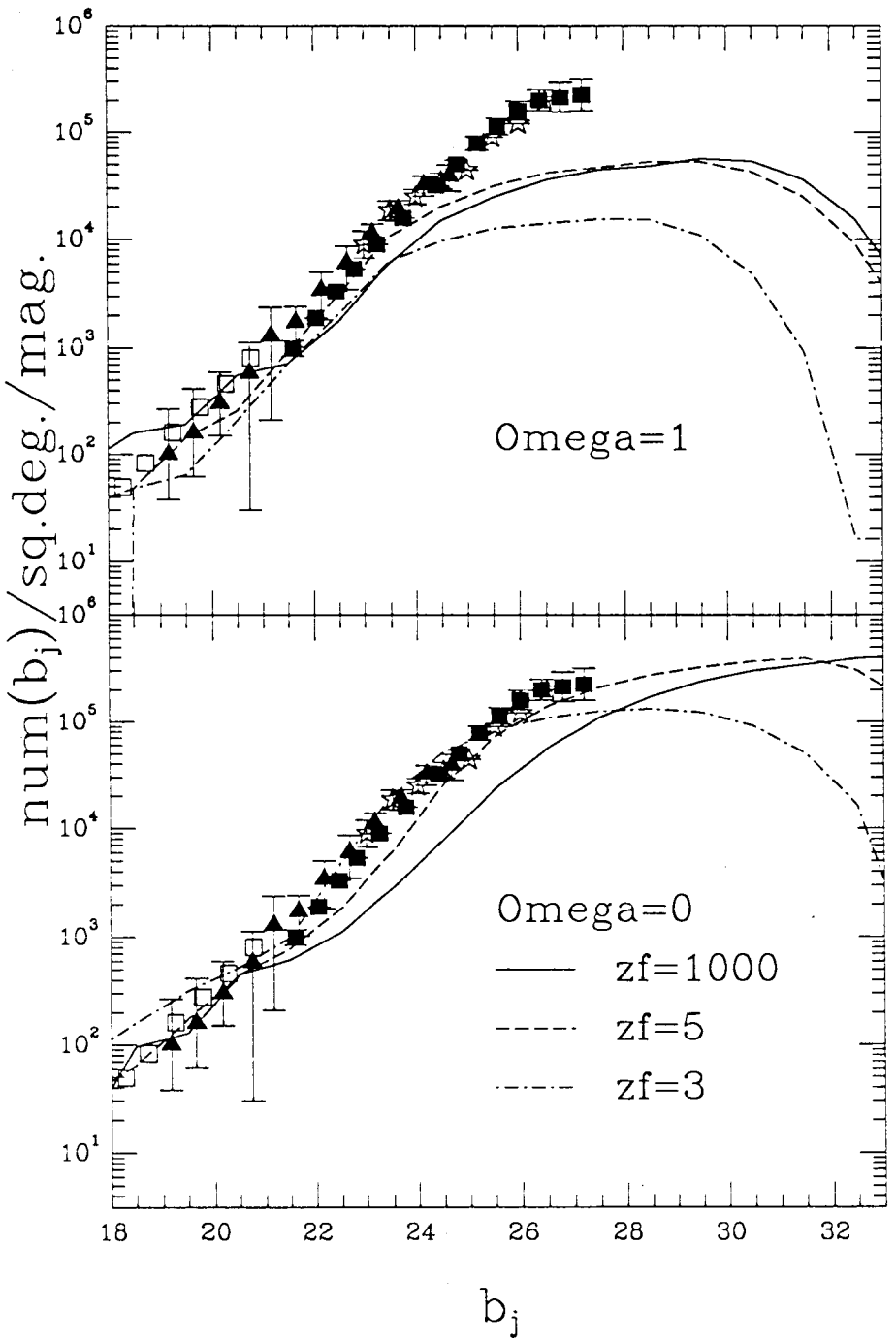
num(b_j)/sq.deg./mag.
Omega=1
Omega=0
zf=1000
zf=5
zf=3
b_j

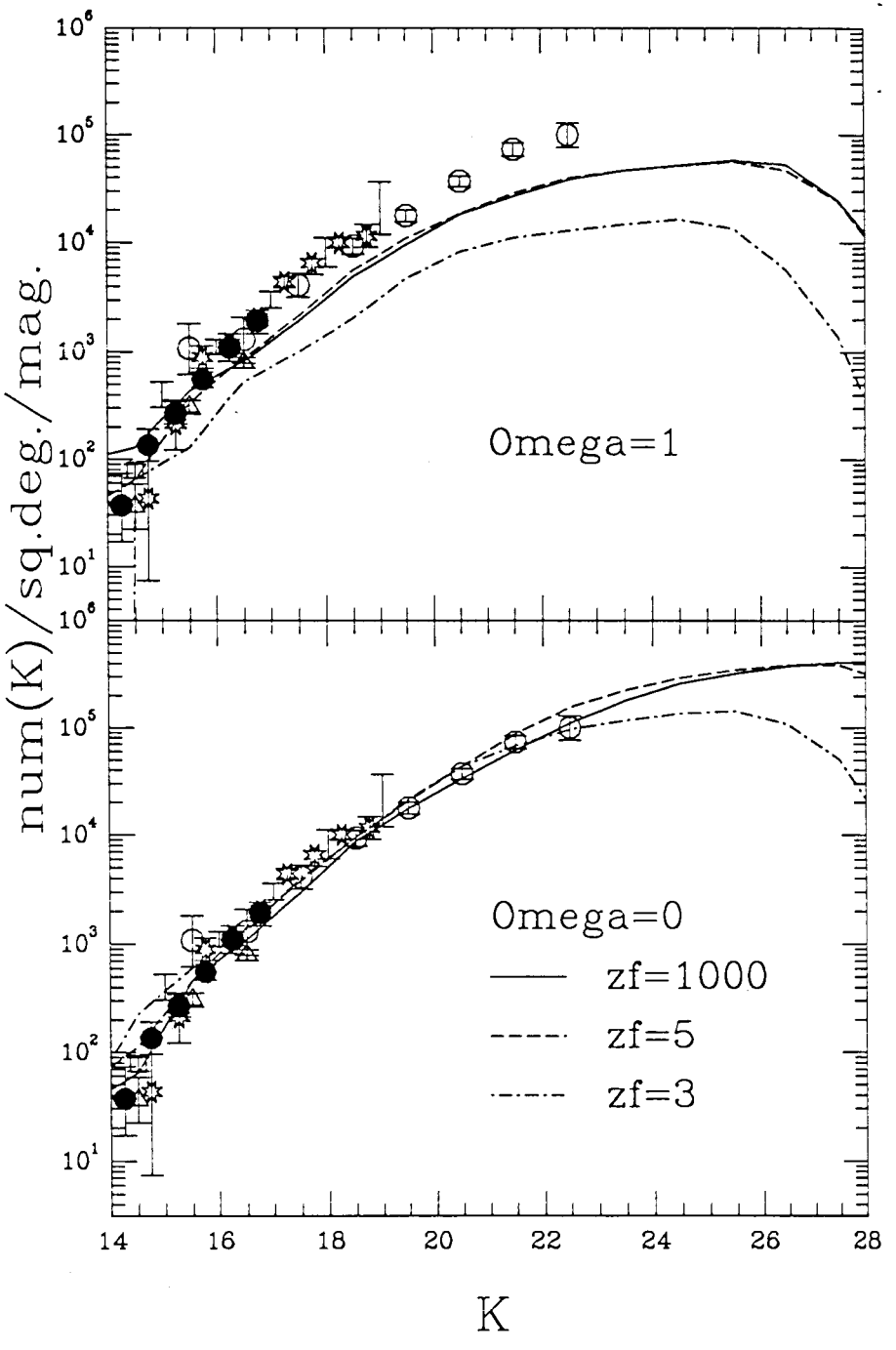
num(K)/sq.deg./mag.
Omega=1
Omega=0
zf=1000
zf=5
zf=3
K

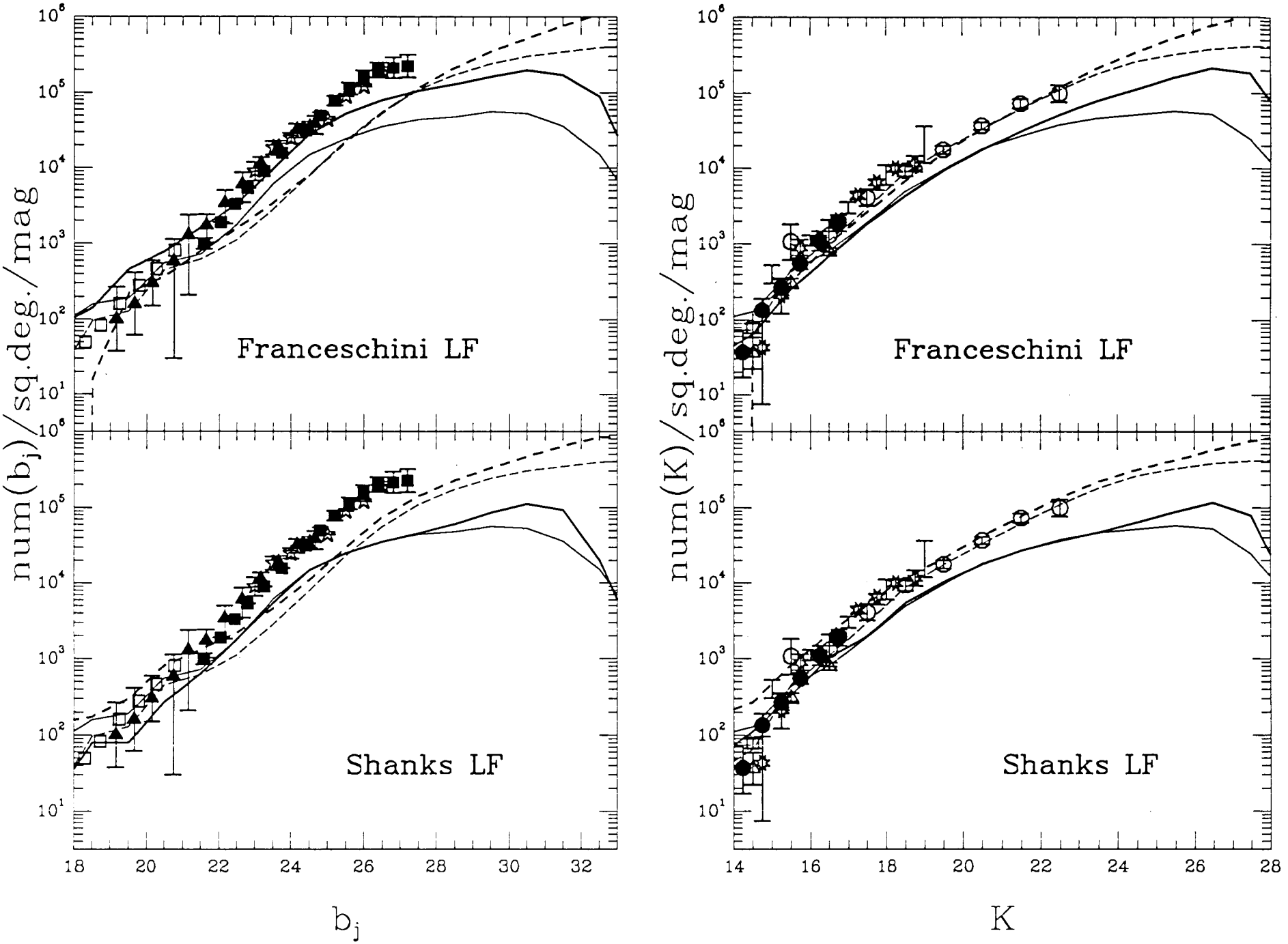
num(b_j)/sq.deg./mag
Franceschini LF
Shanks LF
b_j
num(K)/sq.deg./mag
Franceschini LF
Shanks LF
K

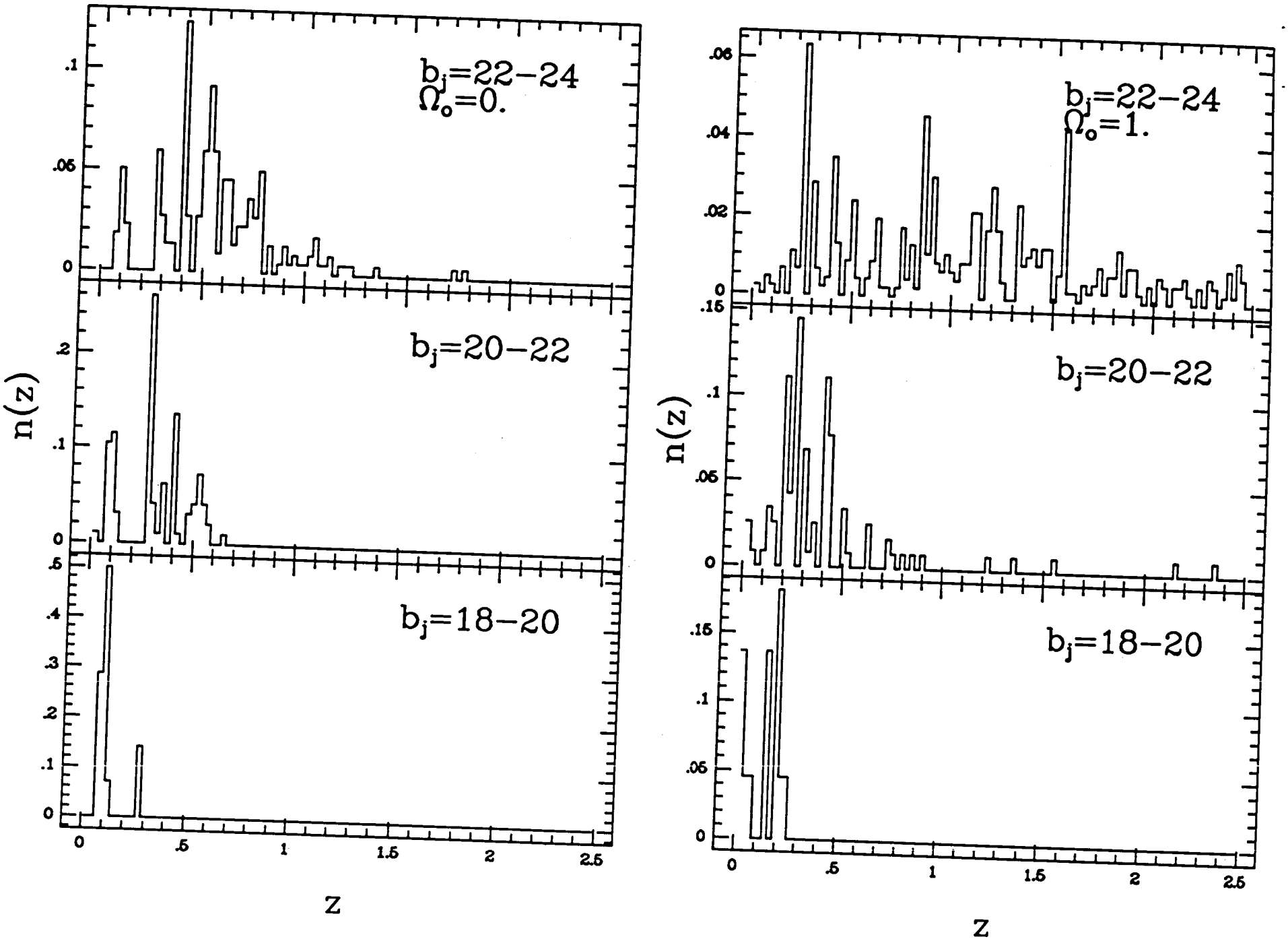
b_j=22–24
Ω_o=0.
b_j=20–22
b_j=18–20
n(z)
z
b_j=22–24
Ω_o=1.
b_j=20–22
b_j=18–20
n(z)
z

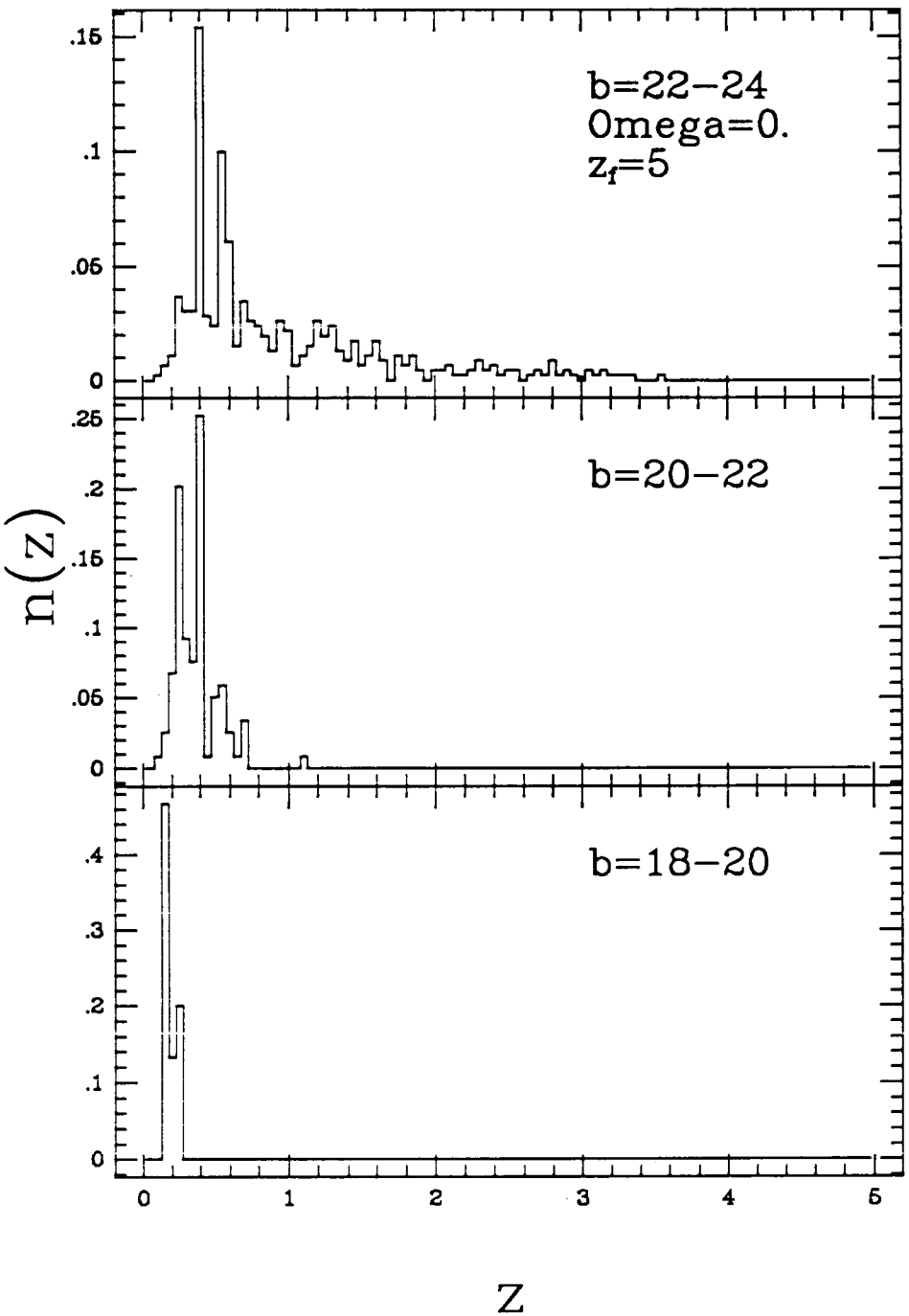
b=22–24
Omega=0.
z_f=5
b=20–22
b=18–20
n(z)
z

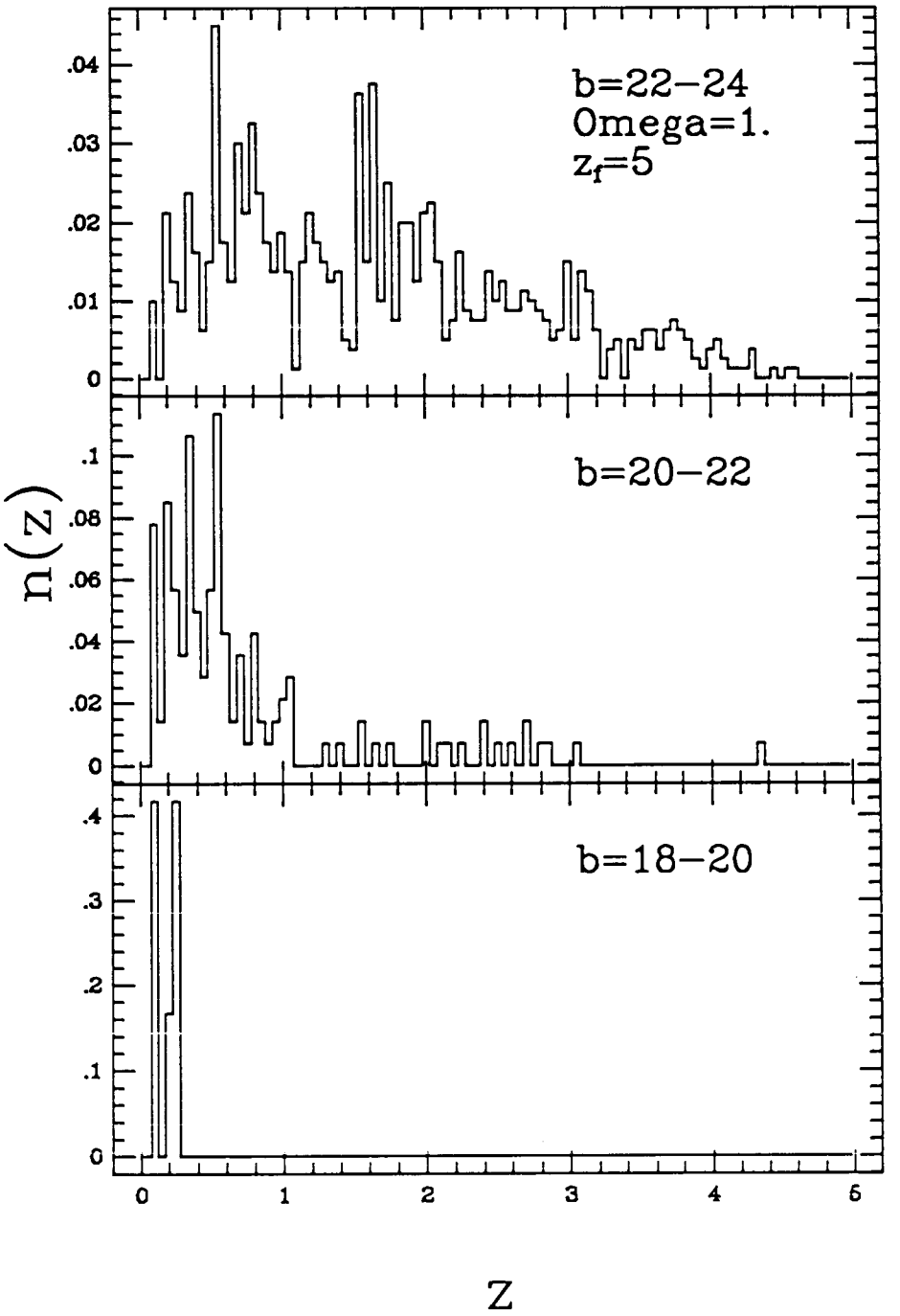
b=22–24
Omega=1.
z_f=5
b=20–22
b=18–20
n(z)
z

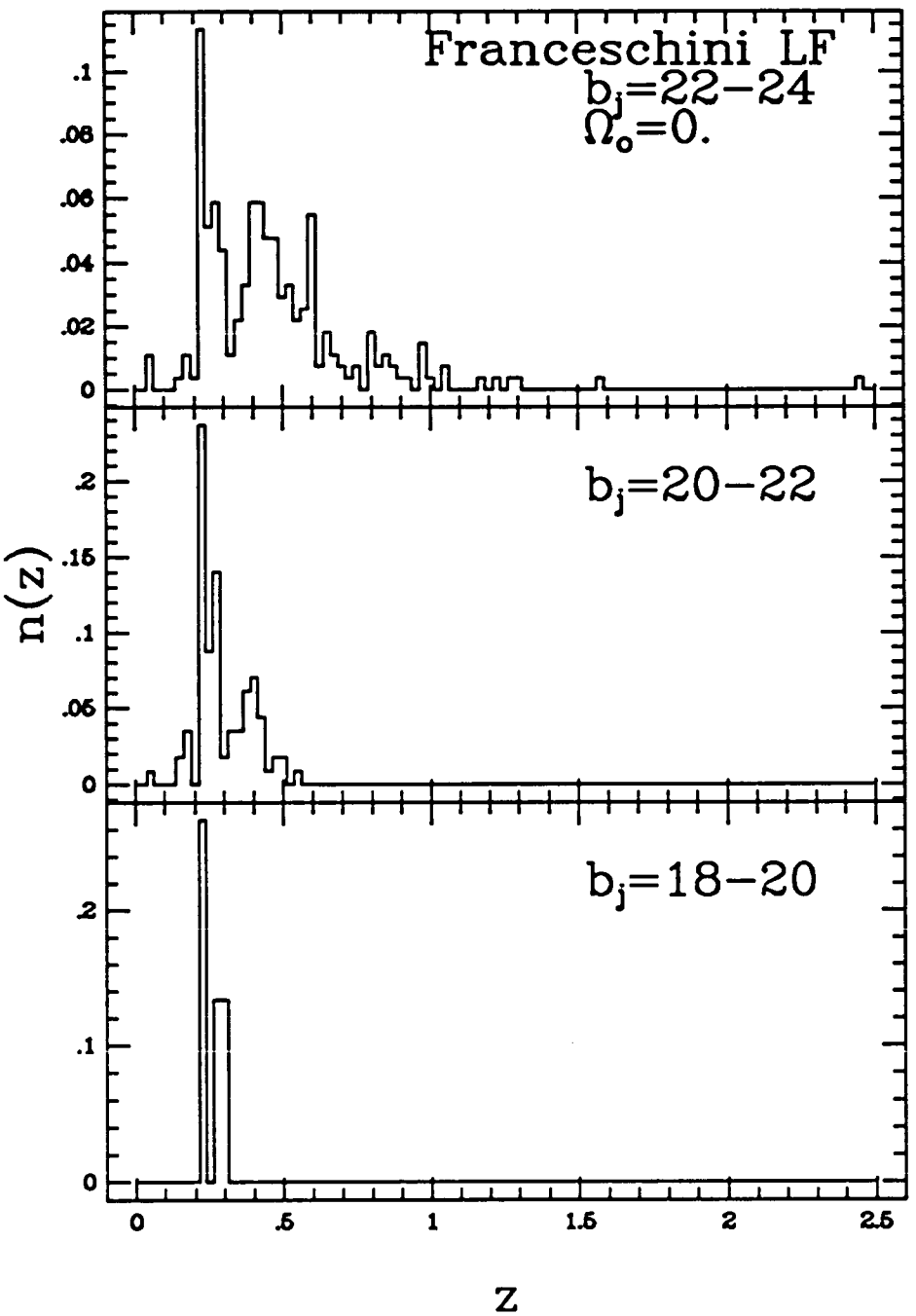
Franceschini LF
b_j=22−24
Ω_o=0.
b_j=20−22
b_j=18−20
n(z)
z

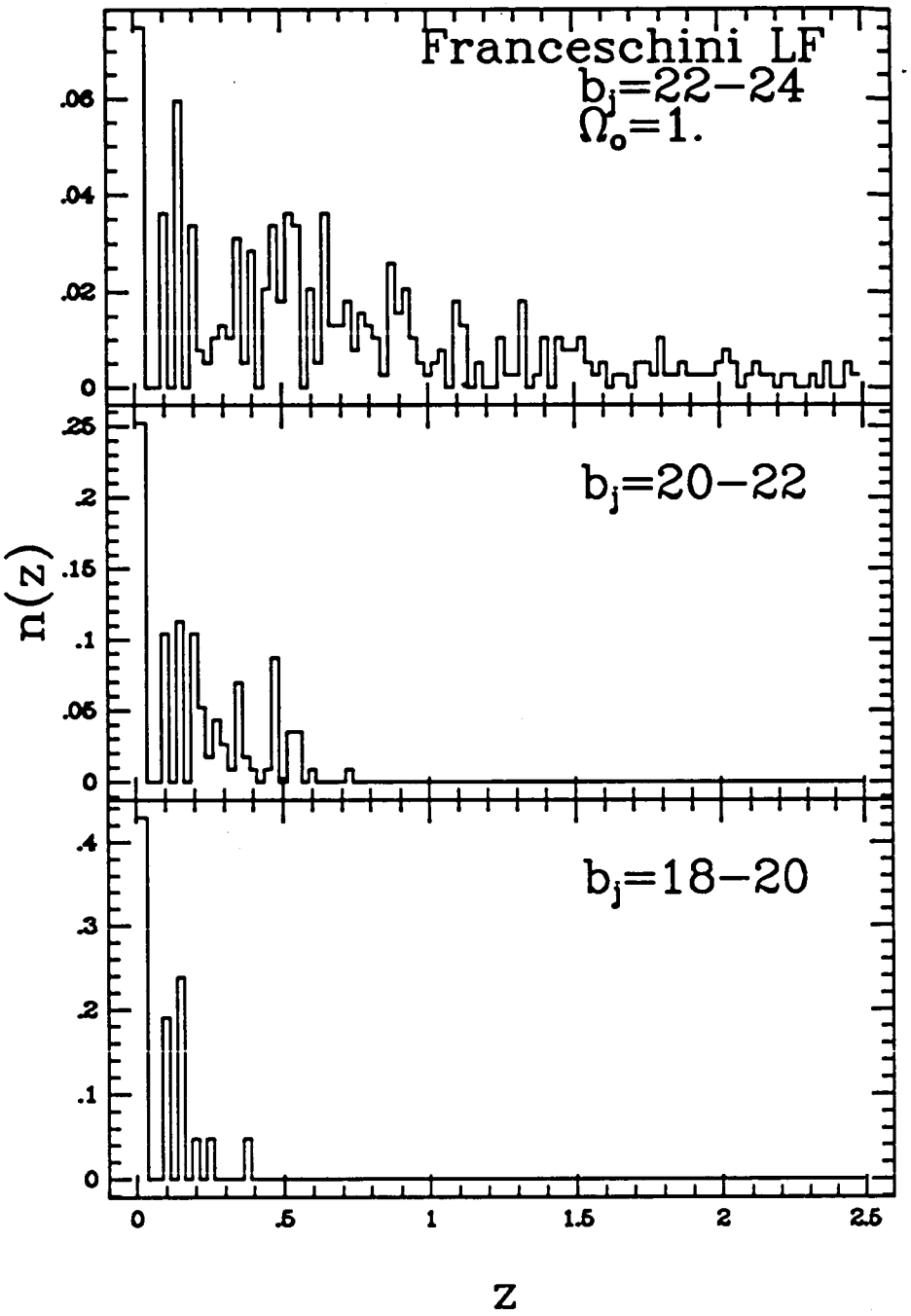
Franceschini LF
b_j=22−24
Ω_o=1.
b_j=20−22
b_j=18−20
n(z)
z

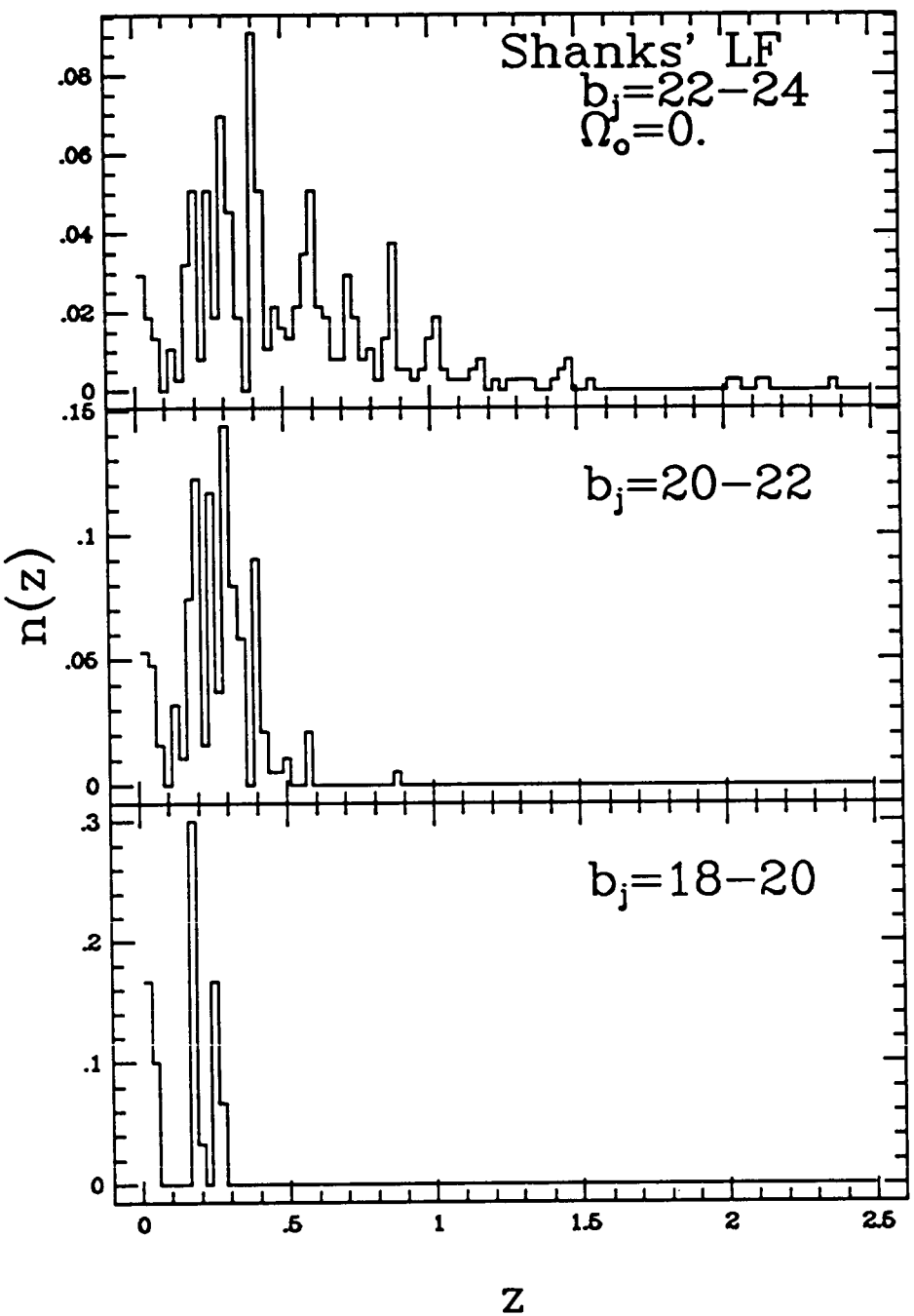
Shanks' LF
b_j=22–24
Ω_o=0.
b_j=20–22
b_j=18–20
n(z)
z

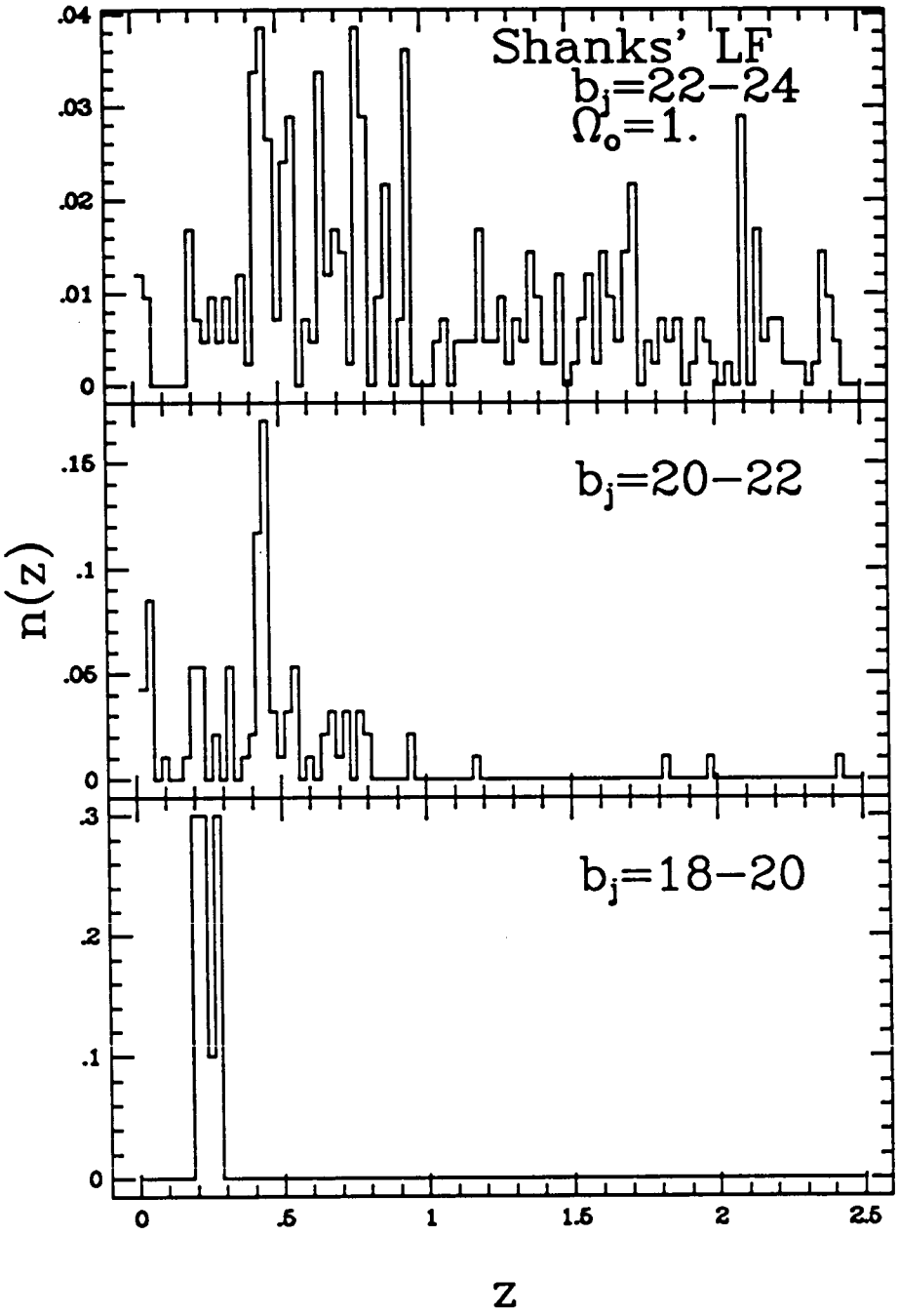
Shanks' LF
b_j=22–24
Ω_o=1.
b_j=20–22
b_j=18–20
n(z)
z

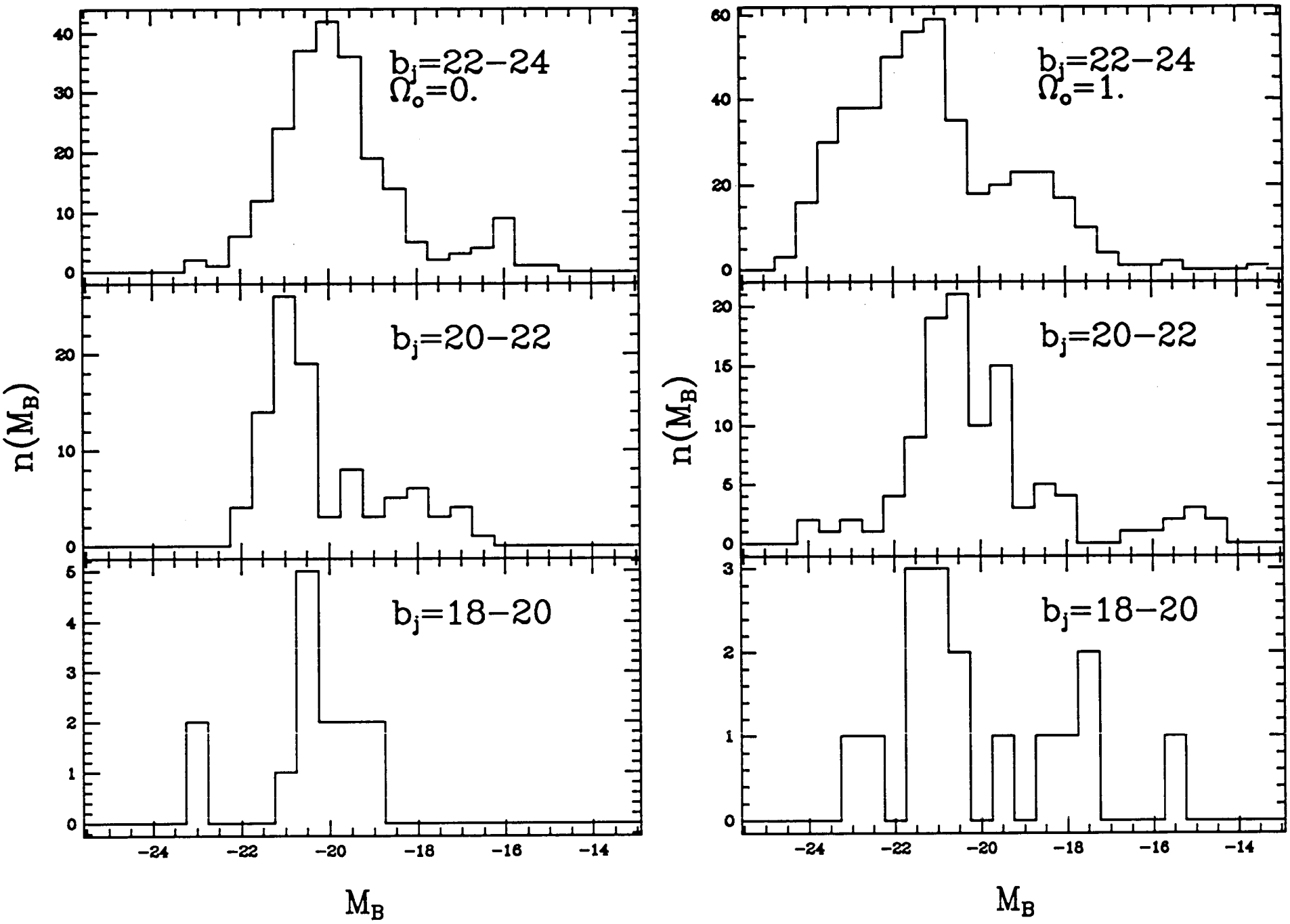
b_j=22−24
Ω_o=0.
b_j=20−22
b_j=18−20
n(M_B)
M_B
b_j=22−24
Ω_o=1.
b_j=20−22
b_j=18−20
n(M_B)
M_B

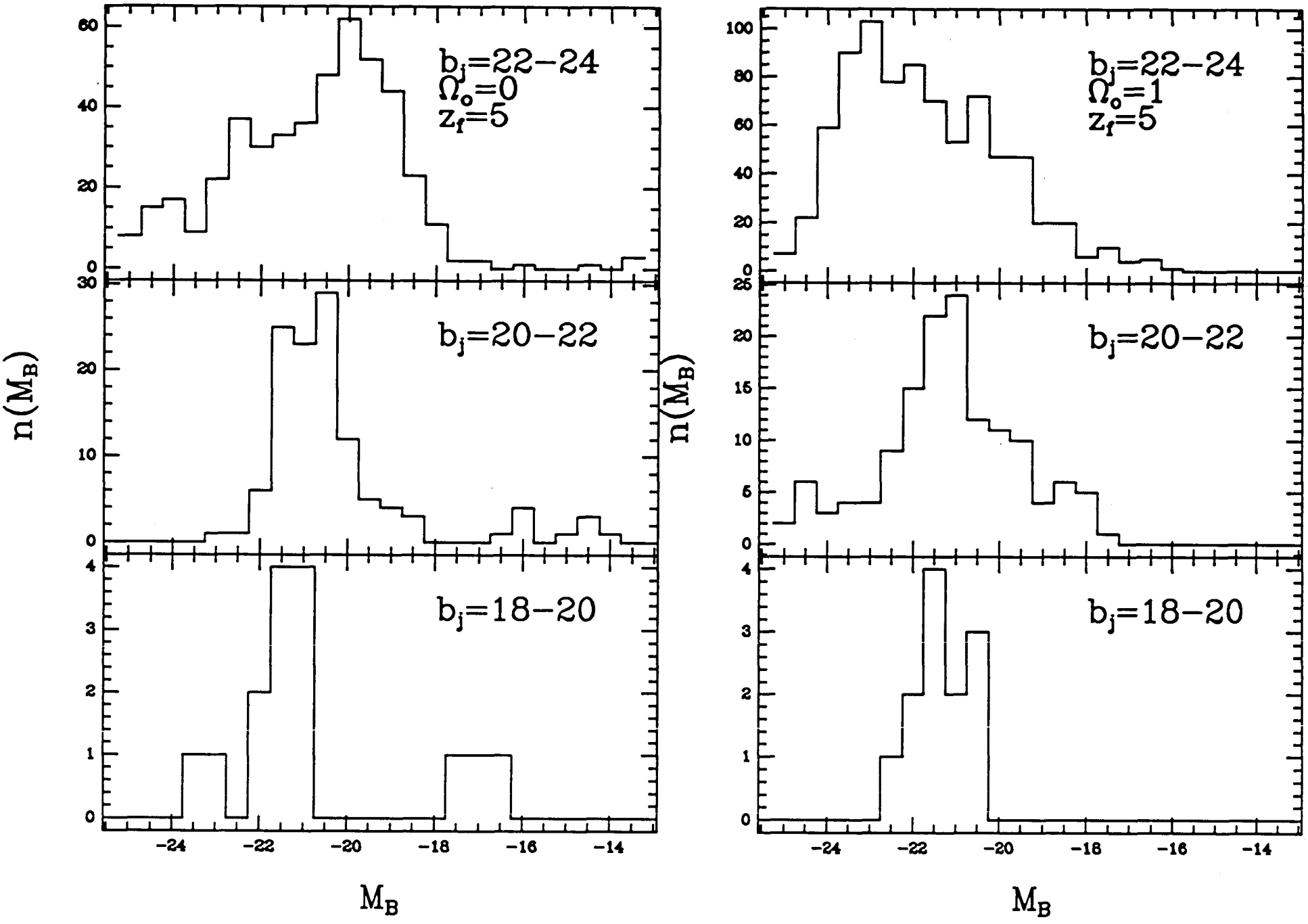
b_j=22-24
Ω_o=0
z_f=5
b_j=20-22
b_j=18-20
n(M_B)
M_B
b_j=22-24
Ω_o=1
z_f=5
b_j=20-22
b_j=18-20
n(M_B)
M_B

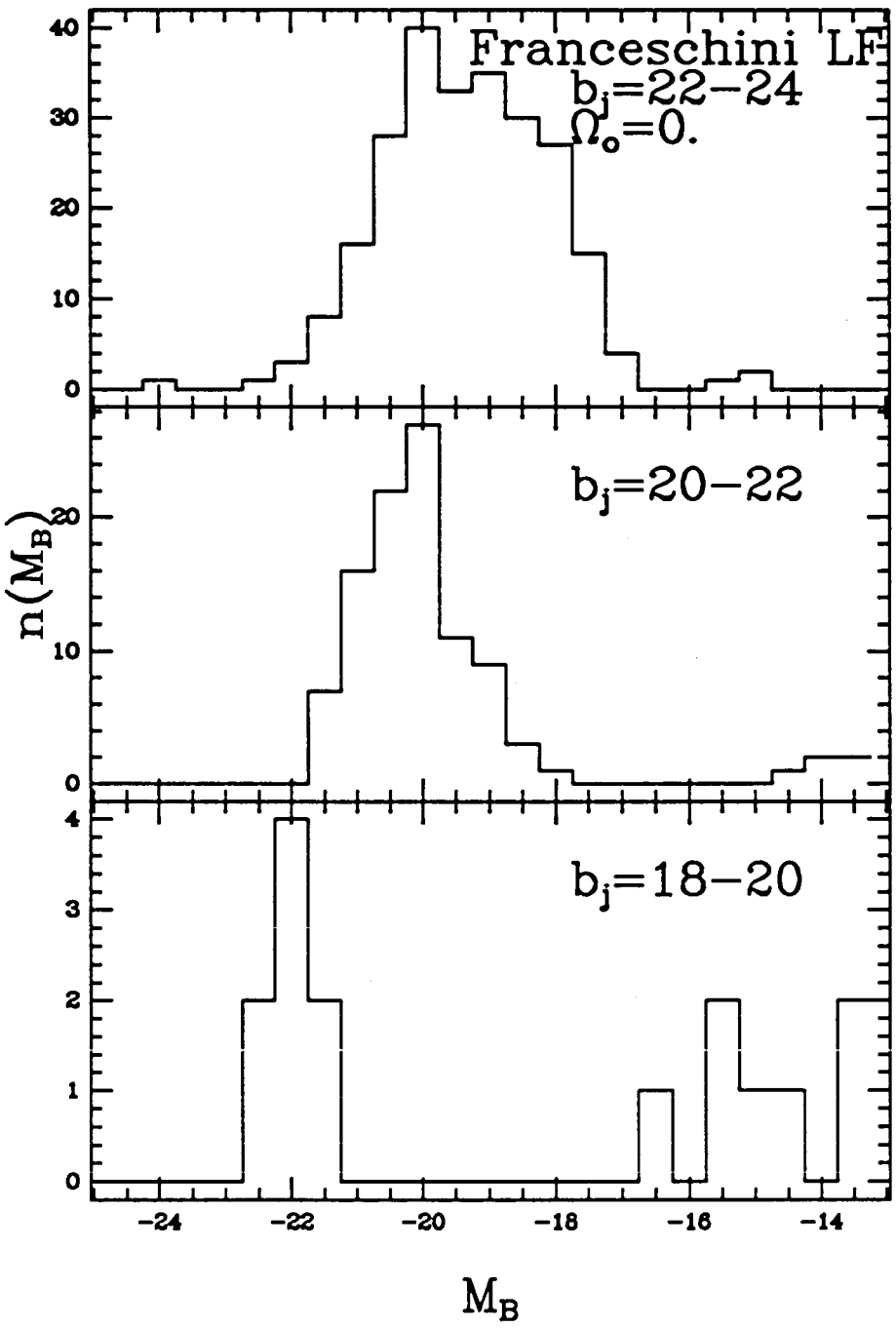
Franceschini LF
b_j=22−24
Ω_o=0.
b_j=20−22
b_j=18−20
$n(M_B)$
M_B

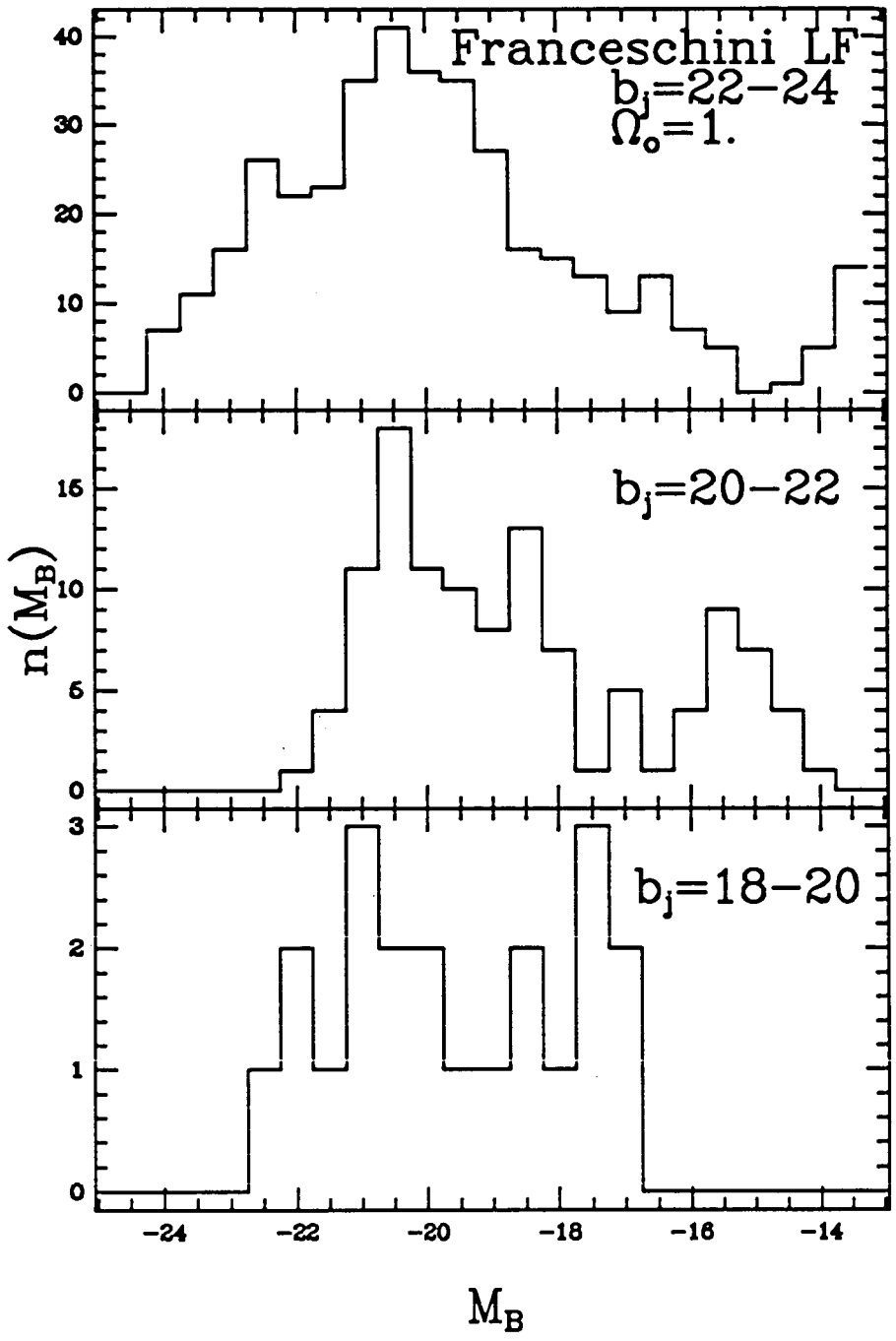
Franceschini LF
b_j=22−24
Ω_o=1.
b_j=20−22
b_j=18−20
$n(M_B)$
M_B

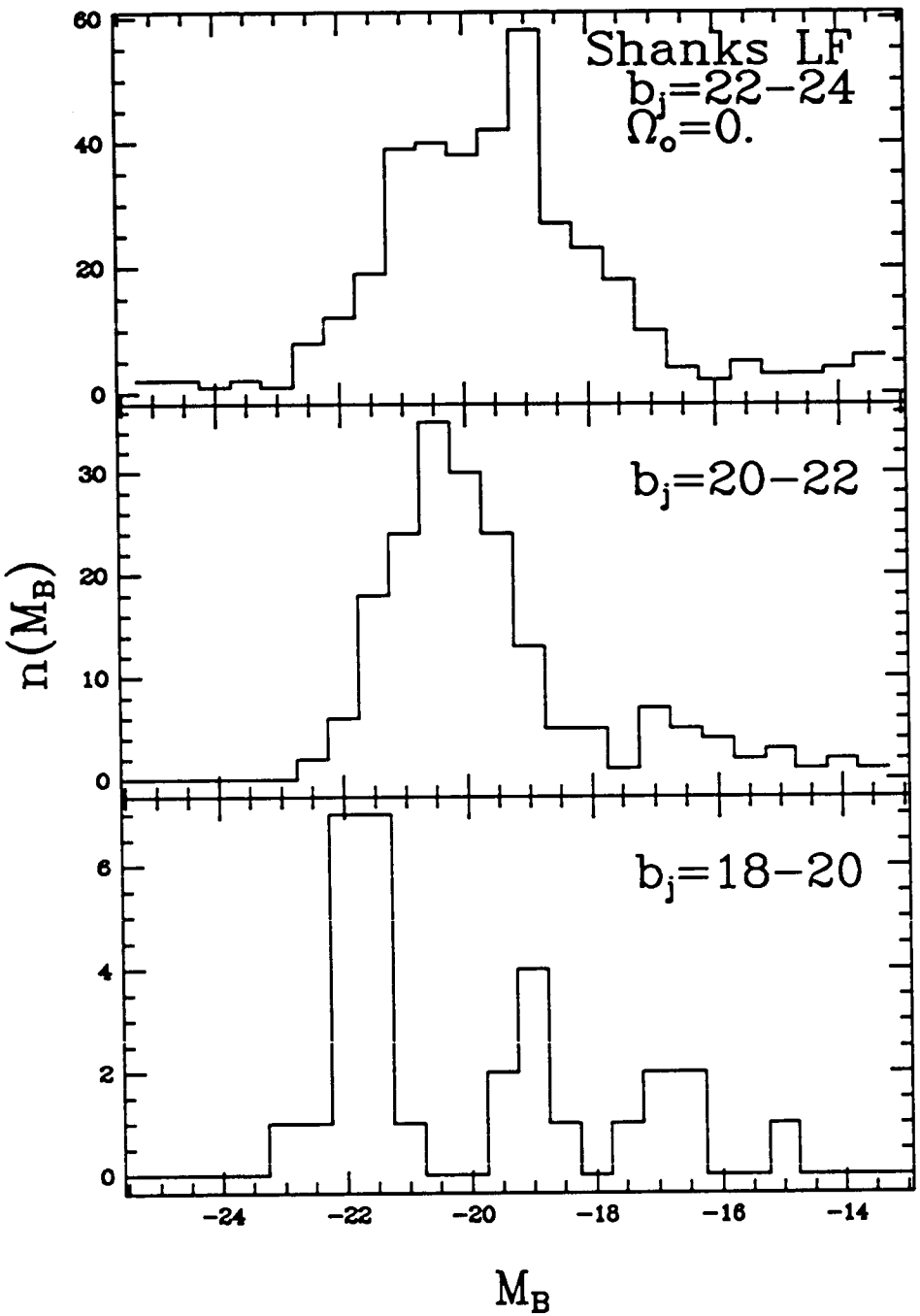
Shanks LF
b_j=22–24
Ω_o=0.
b_j=20–22
b_j=18–20
n(M_B)
M_B

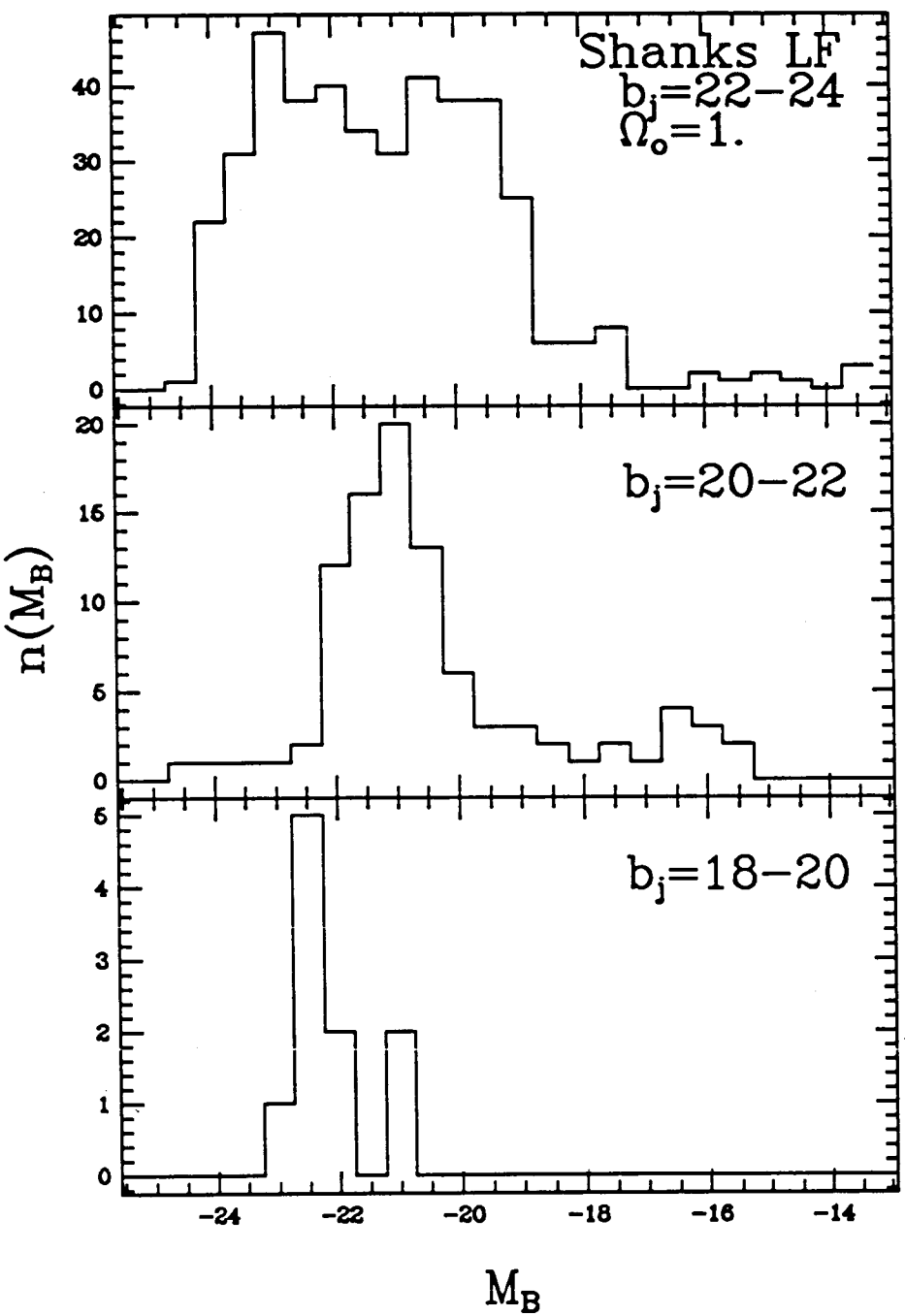
Shanks LF
b_j=22–24
Ω_o=1.
b_j=20–22
b_j=18–20
n(M_B)
M_B

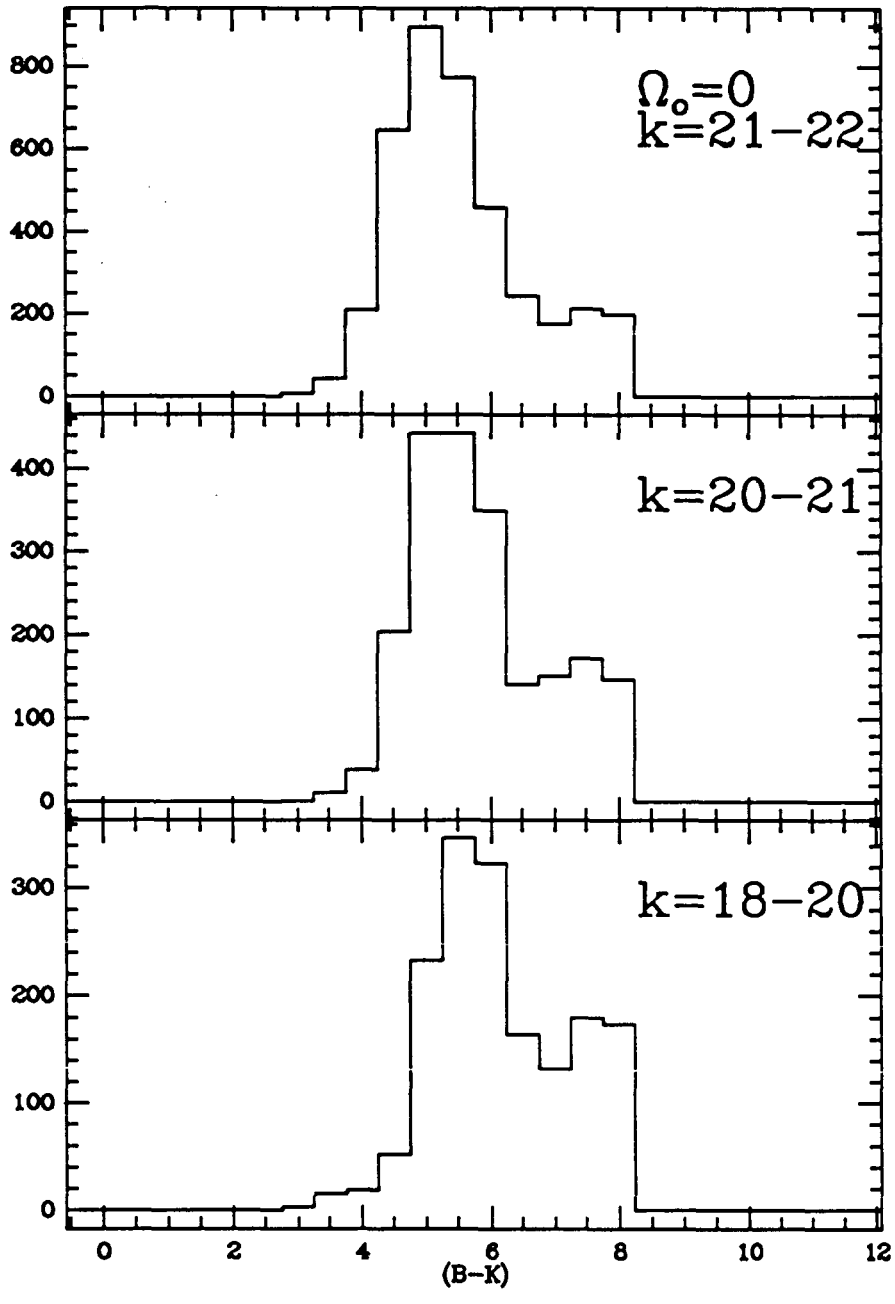
Ω_o=0
k=21−22
k=20−21
k=18−20
(B−K)

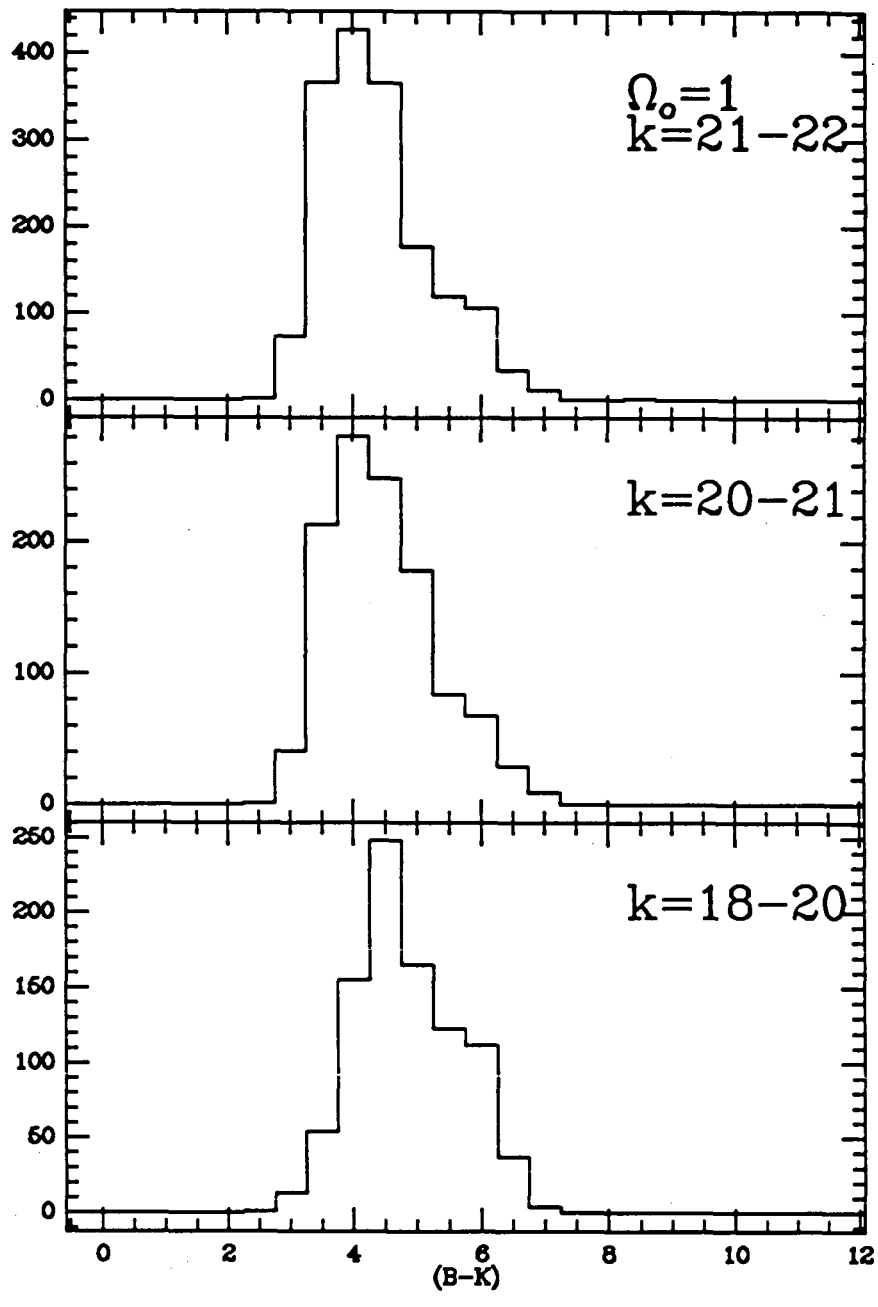
Ω_o=1
k=21−22
k=20−21
k=18−20
(B−K)

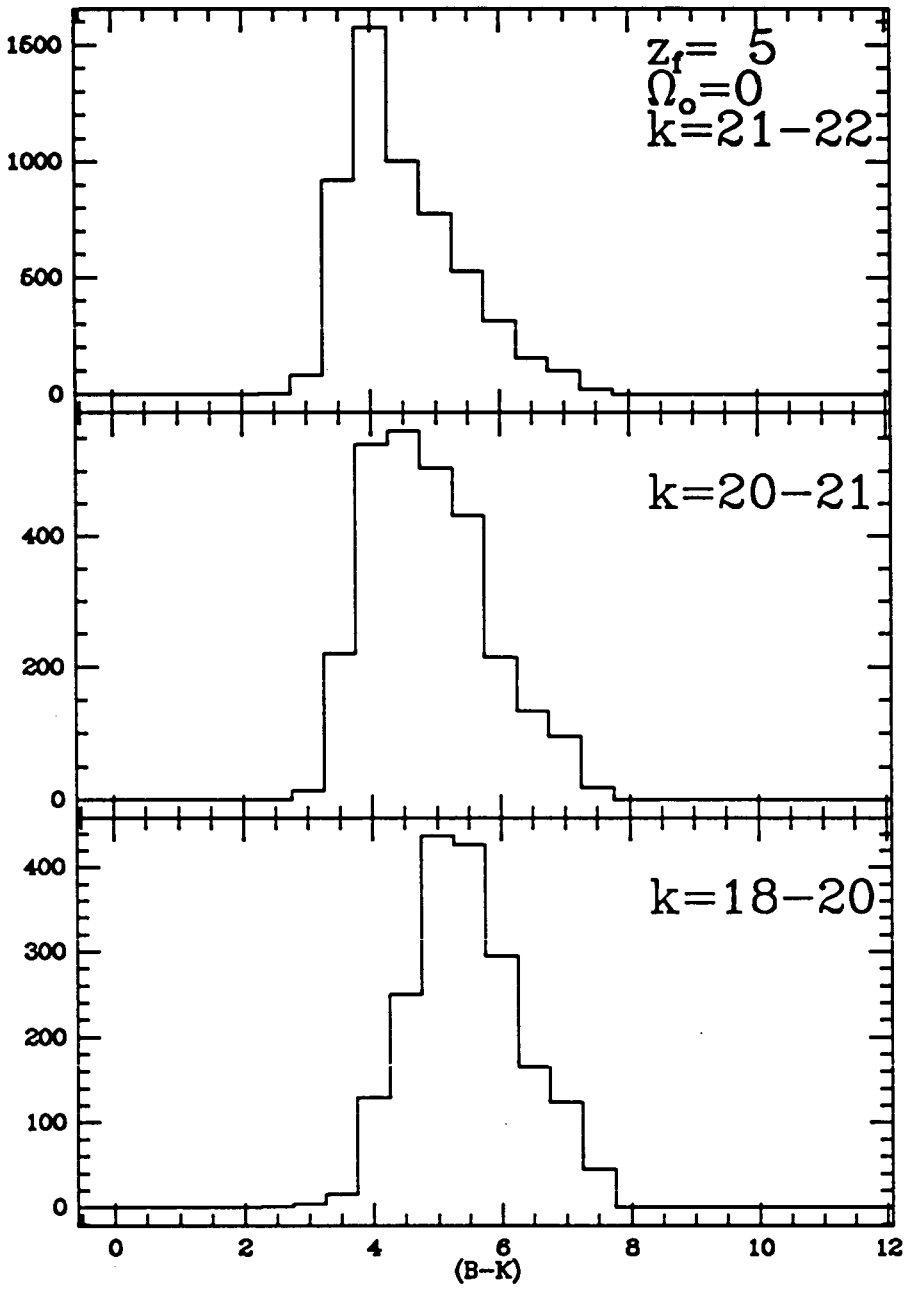
z_f= 5
Ω_o=0
k=21−22
k=20−21
k=18−20
(B−K)

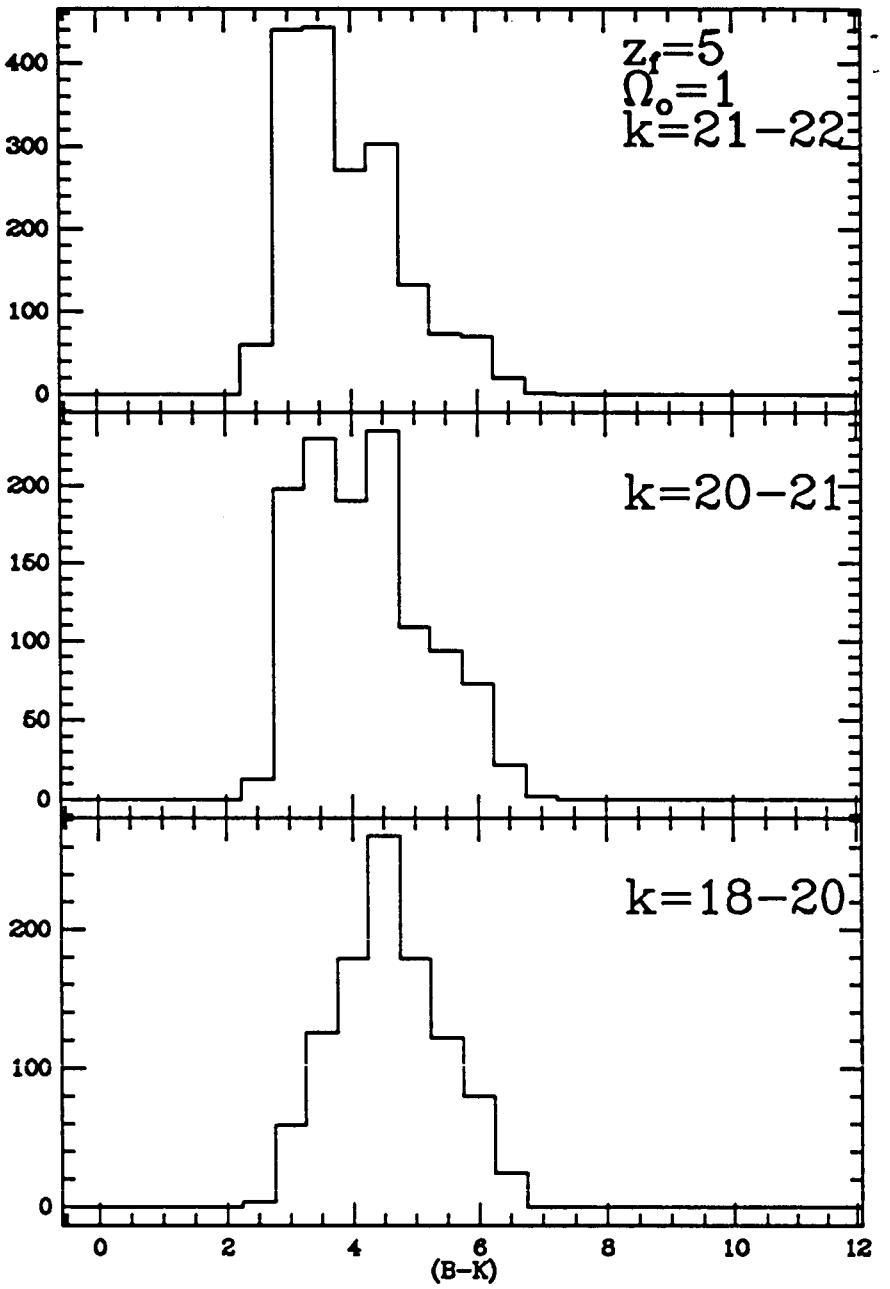
z_f=5
Ω_o=1
k=21−22
k=20−21
k=18−20
(B−K)

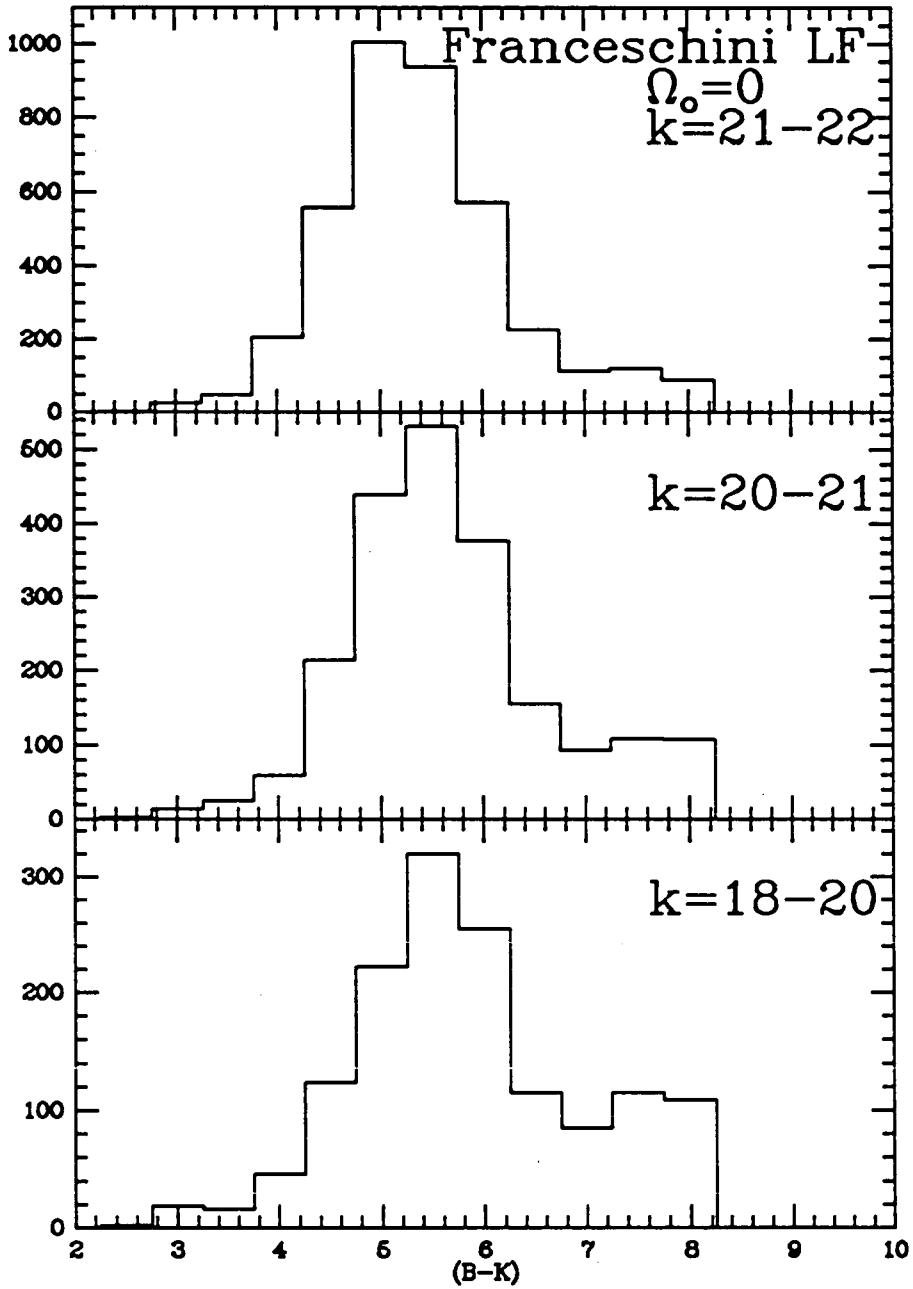
Franceschini LF
Ω_o=0
k=21−22
k=20−21
k=18−20
(B−K)

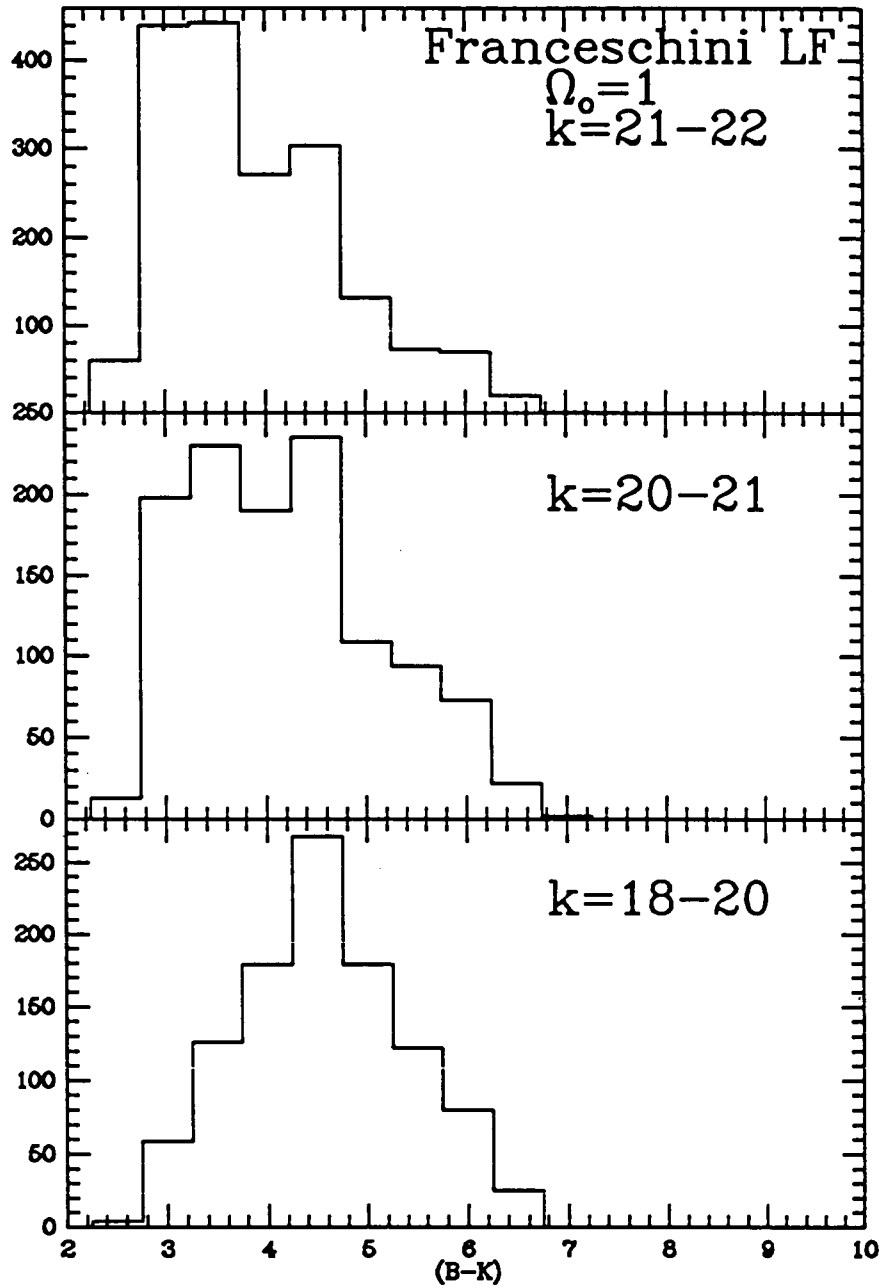
Franceschini LF
Ω_o=1
k=21−22
k=20−21
k=18−20
(B−K)

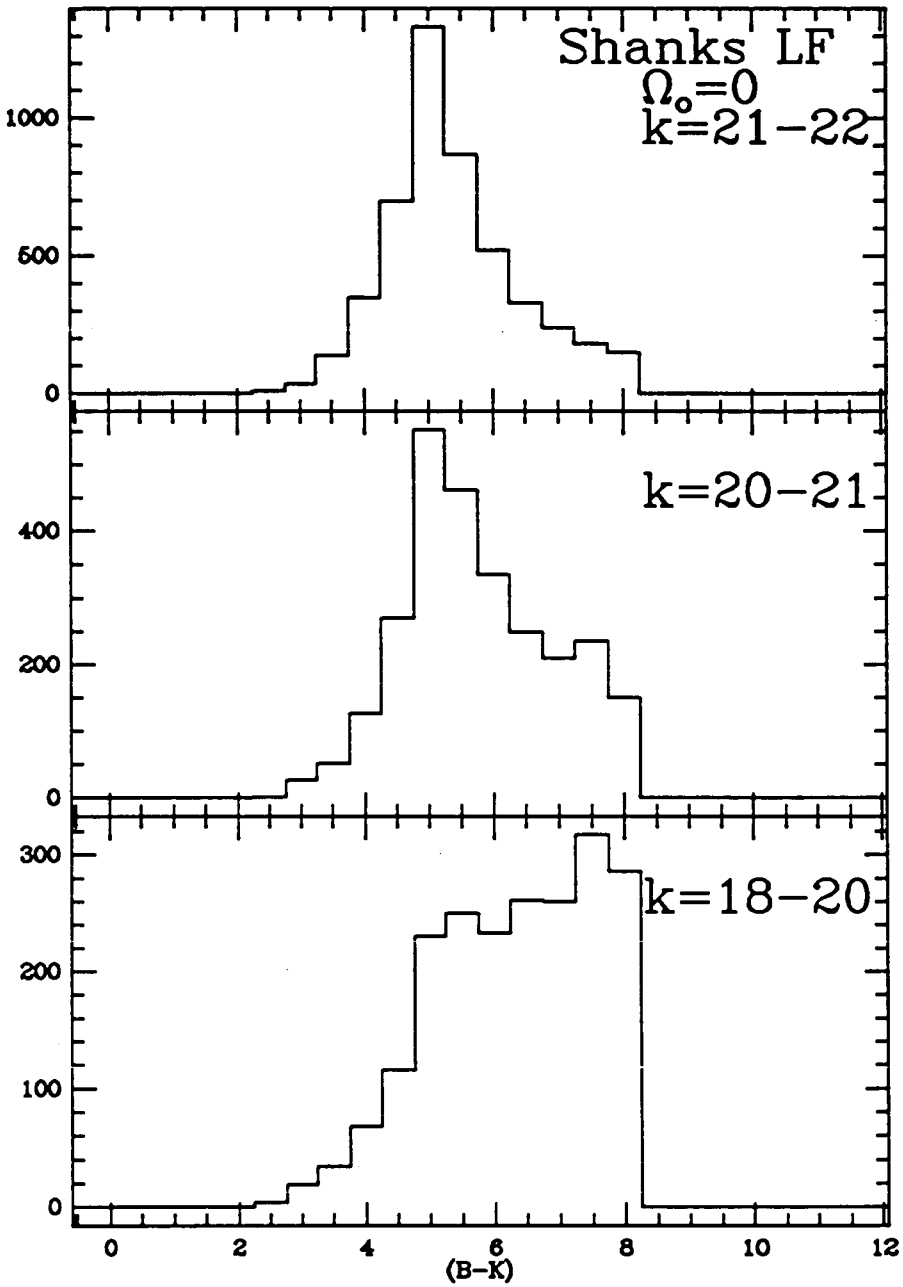
Shanks LF
Ω_o=0
k=21-22
k=20-21
k=18-20
(B-K)

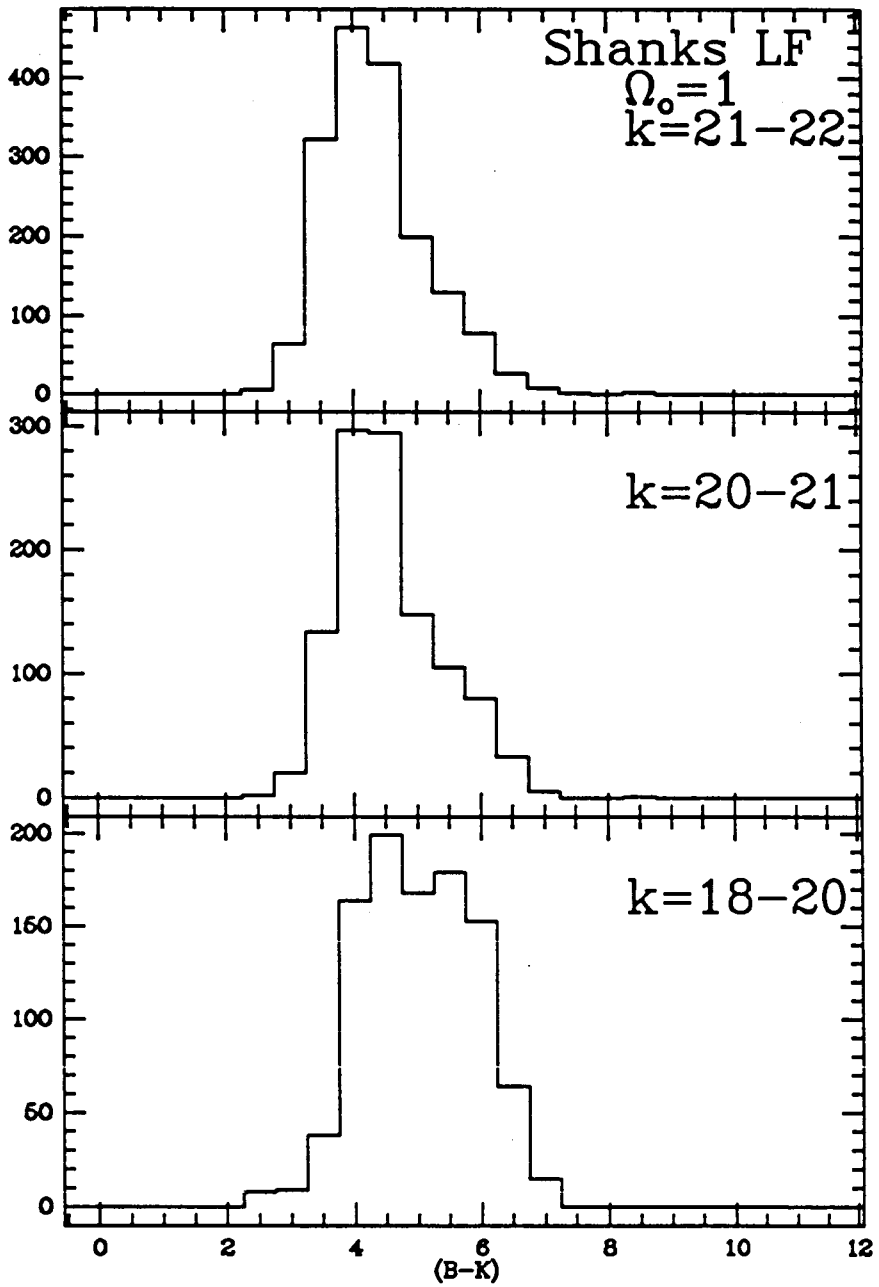
Shanks LF
Ω_o=1
k=21-22
k=20-21
k=18-20
(B-K)

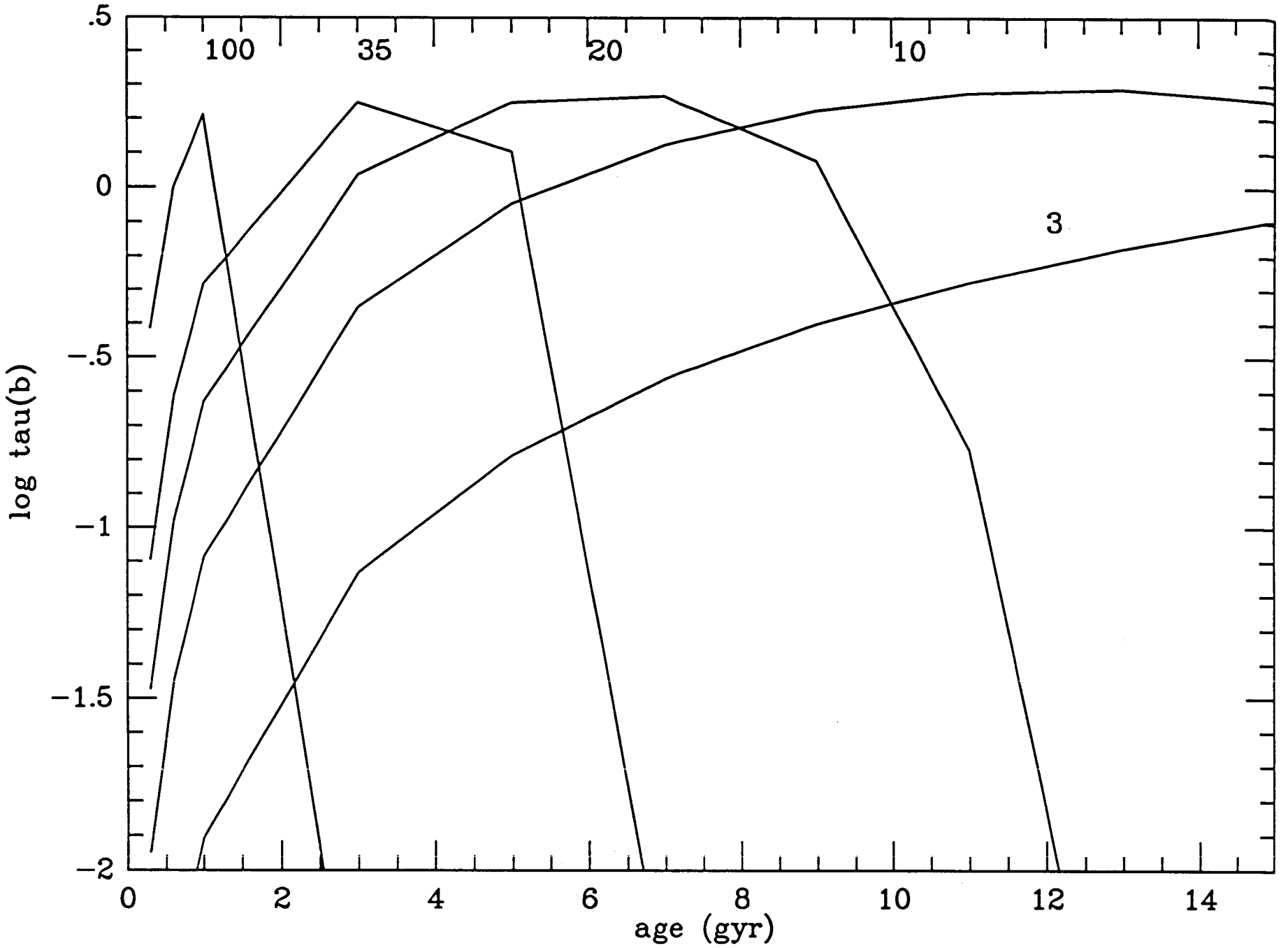
.5
100
35
20
10
0
−.5
−1
−1.5
−2
log tau(b)
3
0
2
4
6
8
10
12
14
age (gyr)